Building and Environment 243 (2023) 110655

Contents lists available at ScienceDirect

Building and Environment

journal homepage: www.elsevier.com/locate/buildenv

Retrofit optimization of building systems for future climates using an urban physics model

Amir A. Aliabadi [a,*,1], Xuan Chen [b,*,1], Jiachuan Yang [b], Ali Madadizadeh [a], Kamran Siddiqui [c]

[a] School of Engineering, University of Guelph, Guelph, Ontario, Canada
[b] Department of Civil and Environmental Engineering, Hong Kong University of Science and Technology, Hong Kong, China
[c] Department of Mechanical and Materials Engineering, Western University, London, Ontario, Canada

ARTICLE INFO

Dataset link: https://www.aaa-scientists.com/, https://github.com/AmirAAliabadi

Keywords:
Building systems
Climate change
Micro-genetic optimization
Renewable and alternative energy
Urban Physics Modeling (UPM)

ABSTRACT

To guide building system retrofits for reducing building's operational carbon footprint, a micro-genetic optimization algorithm has been applied. The algorithm is integrated into the Vertical City Weather Generator (VCWG) urban physics model. The model is applied to low-rise residential houses of Toronto, a cold Canadian city, for annual estimations and reductions of electricity/gas consumption and retrofit cost from 2020 to 2100, every decade, under two Representative Concentration Pathway (RCP) climate change scenarios. The building system configuration utilizes a solar thermal collector, photovoltaic collector, wind turbine, building thermal energy storage, and heat pump. Fifteen building variables have been optimized. Compared to a base building, the proposed retrofitted system reduces the electricity consumption by up to 61.71 [%] and the gas consumption by up to 82.67 [%]. The annualized retrofit cost for a 20-year time horizon is about 10-15 thousand Dollars. Some optimized variables are sensitive to the climate change scenario over a long time horizon until 2100, which relate to the thermal energy storage system, phase change material, solar thermal collectors (and the associated working fluid flow rates), solar heat gain coefficient, and roof albedo. Other variables, relating to the ventilation/infiltration rates, building envelop thermal resistance, glazing ratio, wind turbine size, and photovoltaic collectors, do not show such sensitivity. The optimization process is computationally fast, and the solution obtained provides evidence for successful building system retrofits toward energy and cost savings for the climate of Toronto.

1. Introduction

Buildings are known to consume close to 40 [%] of global energy in the developed world [1]. Under a changing climate with global warming and temperature rises (+0.5 to +3.5 [K] from 1986–2016 to the end of century in 2100), such energy dependence may even exacerbate further in the future [2]. To fight buildings' consequential impact on the climate (via the emissions of GreenHouse Gases (GHGs)), many policy makers, practitioners, and other stake holders advocate for energy retrofits to divert the buildings' dependence on fossil fuels or the GHG emissions associated with the grid electricity. Such retrofits target the reduction of GHG emissions via reducing the operational carbon footprint of buildings. The retrofits typically involve an initial investment in improving the existing building systems (such as envelop thermal performance, air tightness, high efficiency boilers/furnaces, etc.) or installation of new renewable/alternative energy systems (such as photovoltaics/solar thermal collectors, heat pumps, thermal energy storage, etc.). The resulting energy savings for the retrofitted system will reduce the GHG emissions, and the investment is characterized with an annualized cost.

It is noteworthy to mention that building system retrofits usually target the reduction of *operational* carbon emissions, as opposed to *embodied* carbon emissions. Consideration of embodied carbon emissions are more relevant for construction of new buildings, where choices of the land use modification, use of construction materials, construction methods, and building systems determine the embodied carbon footprint. In fact, there are tradeoffs between operational and embodied carbon emissions of buildings [3].

Building retrofits present an underlying optimization problem. On the one hand, a retrofitted building will achieve energy savings, which should be maximized; on the other hand, an initial investment is required for the retrofit, which should be minimized. The optimization process shall find the most cost-effective way to save the greatest

* Corresponding authors.
E-mail addresses: aliabadi@uoguelph.ca (A.A. Aliabadi), cxlne.xuan.chen@connect.ust.hk (X. Chen).
URLs: https://www.aaa-scientists.com (A.A. Aliabadi), https://cejcyang.people.ust.hk/ (X. Chen).
[1] These authors contributed equally.

https://doi.org/10.1016/j.buildenv.2023.110655
Received 19 May 2023; Received in revised form 12 July 2023; Accepted 20 July 2023
Available online 26 July 2023

amount of energy consumption. This presents a challenge in retrofit studies, which is the selection and sizing of building systems that result in cost-effective energy savings [4,5]. Buildings are characterized with too many variables and systems. Any modeling study that attempts to find the absolutely best set of systems and variables will soon find itself too computationally expensive, as there is a large set of variable permutations necessary for such a model. For instance, consider 5 building features to be optimized and that each building feature can adopt 5 values. This demands $5^5 = 3125$ simulations to try all the permutations. This highlights the importance of effective optimization methods for building system retrofit studies.

1.1. Review of building optimization techniques

We provide a brief and selective review of building optimization algorithms investigated during the past 20 years. The landmark study by Wetter and Wright [6] performed numerical experiments on three groups of algorithms: (1) direct search, (2) stochastic population-based, and (3) gradient-based algorithms. It was understood since then that direct search and gradient-based algorithms often fail for building optimization problems, in which the objective function(s) have discontinuities. The following studies for the next 2 decades focused on stochastic population-based algorithms. The key trade off for such algorithms is between the computational cost (i.e. number of iterations) and the probability that a nearly global optimum solution is found. Yet, convergence to a global optimum solution cannot be established formally for such methods [7].

A common optimization technique is to transform a set of objective functions (e.g. electricity consumption, gas consumption, and cost) to a single overall objective function using the weighted sum approach [5,8–10]. Then the overall objective function may be minimized using variations of stochastic population-based algorithms such as particle swarm [11], ant colony [9,10], or evolutionary [12] algorithms. The majority of optimization studies use the EnergyPlus building scale model for their investigations.

In the Particle Swarm Optimization (PSO) methods, an optimum solution is found by iterative movement of a population of solutions (particles) along the search space, for which the movement is characterized by each particle's position and velocity. Each particle's motion is influenced by its best known local position though it is also maneuvered toward the best known positions in the entire search space. These best positions are updated as better positions are found by other particles. It is expected that particles will gradually move toward the best positions (solutions). Building PSO algorithms explored by Wetter and Wright [6] involved 16 particles and 20 generations. They required up to 195–712 iterations to optimize a problem with 13 variables. They showed the best reduction in the objective function but required a large number of iterations. Hybrid PSO algorithms are sometimes combined with search methods (such as the Hook Jeeves (HJ)). PSO-HJ methods use PSO as the main search algorithm, which is then refined to approach the global optimum using the HJ algorithm [7]. Wetter and Wright [6] found these algorithms requiring 653–889 iterations. Building PSO-HJ algorithm explored by Kämpf et al. [7] required close to 3400 iterations to optimize 13 variables. Building PSO-HJ algorithms explored by Bamdad et al. [9,10] required up to 4000 iterations to optimize 9 variables.

In the ant colony optimization methods, artificial ants (i.e. simulation agents) locate optimum solutions by moving through the variable space that represents all potential solutions. Real ants lay traces to direct each other to resources (e.g. food) while exploring the natural environment. The simulated ants likewise record their positions and the quality of the solutions, so in later simulations more ants locate themselves for better solutions. The algorithm aims to search for an optimal path in a graph, based on the behavior of ants seeking a path between their colony and a resource of food. For building optimizations, the Ant Colony Optimization algorithm for Mixed Variables (ACOMV) has been developed [9,10]. Ant colony optimization methods are suggested to be 50 [%] faster than particle swarm optimization methods, but they still require many iterations, up to 4000 for 9 variables [9].

In the evolutionary optimization methods (Genetic Algorithms (GA)s), mechanisms inspired by biological evolution, such as reproduction, mutation, recombination, and selection are used. Iterative solutions to the optimization problem play the role of individuals in a population, and a fitness function determines the quality of the solutions. The evolution of the population then takes place after the repeated application of the evolutionary mechanisms. The building GA explored by Wetter and Wright [6] required a population of 14 solutions and 50 generations of subsequent solutions. It required up to 853–592 iterations. Wetter and Wright [6] found that GAs could require fewer iterations and yet land near the global optimum solution. However, they may risk not finding a nearly global optimum if their number of iterations are too few. The building GA explored by Kämpf et al. [7] required close to 3000 iterations to optimize 13 variables. The building GA explored by Gunay et al. [13] required a population of 75 solutions and 8 generations (600 iterations) to optimize 8 variables. They suggested that GAs handle problems with multi-modal objective functions better than PSO algorithms, yet GAs can fail if the number of variables reach beyond 20. For building optimizations, Tuhus-Dubrow and Krarti [14] and Bamdad et al. [9] have found that GAs take fewer iterations than PSO methods to find a solution in the proximity of the global optimum. The GA explored by Mukkavaara and Shadram [3] required 4920 iterations to optimize 9 variables. Recently, the micro-genetic optimization method has been proposed that requires fewer iterations for models of high computational cost [12].

1.2. Research gaps

Many building energy studies solely focus on standard building features, such as envelop thermal resistance, glazing ratio, building orientation, ventilation/infiltration rate, and as such for the current and future climates [9–11,15,16]. However, fewer studies explore the selection and sizing of renewable/alternative energy systems, such as photovoltaic/solar thermal collectors, building thermal energy storage systems, phase change materials, heat pumps, and the like, particularly for cold climate of Canada [5,17–23].

Optimization techniques that are based on common particle swarm, ant colony, or genetic methods are generally very computationally expensive [11]. So it is imperative to find alternative stochastic population-based optimization methods that can provide nearly global optimum solutions with fewer iterations.

Typical modeling software used for assessment of building system retrofits are EnergyPlus, Transient System (TRNSYS) simulation tool, and Integrated Environmental Solutions Virtual Environment (IESVE). These tools are effective for assessment of standard building features and alternative/renewable energy systems [24,25]. However, they do not account for the interaction between buildings and the surrounding outdoor conditions with sufficient detail and accuracy (e.g. shading/wind drag effect from other buildings, evapotranspiration from vegetation, and impact of a building's waste heat on its energy consumption). Alternative modeling tools can be used to fill this gap. For instance, the Urban Weather Generator (UWG) [26–29] and the Vertical City Weather Generator (VCWG) [5,30,31] can be used to account for the feedback interaction of a building with the outside environment, considering the exchanges of momentum, energy, and humidity; or the integrated City Fast Fluid Dynamics (CityFFD), an urban-scale fast fluid dynamics model for microclimate modeling, and City Building Energy Model (CityBEM) allow for local exchanges of aerodynamics and heat transfer processes between the two models [32].

1.3. Objectives

This study aims to fill the aforementioned research gaps by a few novel investigations: (1) it attempts to optimize a list of 15 building variables beyond conventional envelop and operating variables (i.e. envelop thermal, glazing, infiltration, and ventilation variables) by including variables pertaining to renewable/alternative energy systems for cold climate (i.e. solar thermal, photovoltaics, wind, and thermal energy storage variables); (2) it employs a comprehensive urban physics model that not only accounts for building scale systems, but also accounts for the feedback interaction of building systems with the outside environment (e.g. presence of other buildings and vegetation) in detail; (3) it applies a micro-genetic optimization algorithm to arrive at a nearly optimum solution much faster than conventional building optimization algorithms.

A typical single-detached low-rise two-storey residential house is considered in the climate of Toronto, Canada. Single-detached residential houses account for 52.6% and 56% of residential building stock in Canada and Ontario, respectively [33]. Further 71% of such houses use natural gas for their heating needs in Ontario [33]. This building type is representative in the Canadian context, while in other countries it may account for a lower or higher fraction of residential building stock. This typical housing stock is far less energy efficient than houses conforming to high standards [34,35]. The poor energy performance can be attributed to key building envelop features. For instance, typical standard thermal resistances in ASHRAE climate zone 5 for walls and roofs are 3.5 and 5.5 [m^2KW^{-1}], while the corresponding values according to the Passive House Institute are 7.0 and 11.5 [m^2KW^{-1}]. Likewise, typical new construction houses in Ontario experience an infiltration rate of 2.5–3.5 [ACH], while the Passive House Institute requires a stringent air tightness of 0.6 [ACH] [36].

The energy consumption of the house is assessed from 2020 to 2100 under two Representative Concentration Pathways (RCPs) of 4.5 and 8.5 [Wm^{-2}]. Ideally, based on the Intergovernmental Panel on Climate Change (IPCC)'s Sixth Assessment Report (AR6), Socioeconomic Pathways (SSPs) should be considered, since they make projections in population, urbanization, rate of technology development, rather than RCPs, that primarily focus on abundance of greenhouse gas emissions [37]. However, many regional climate model data products (including the one used in this study) are presently only available based on the Fifth Assessment Report (AR5)'s RCP scenarios, so RCP scenarios are used in this study.

The Vertical City Weather Generator (VCWG v1.5.0) urban physics model is developed and used with a micro-genetic optimization algorithm to model the residential house by sizing and selecting 15 building variables, including standard building features and renewable/alternative energy systems for the optimization. To force VCWG with weather files, the Vatic Weather File Generator (VWFG v1.0.0) is used. The study performs simulations of annual energy consumption and retrofit cost for every decade from 2020 to 2100 using one representative year for each decade (i.e. for years 2020, 2030, 2040, etc.). The optimized solutions are analyzed and interpreted for their sensitivity to time and the future climate change scenario.

Section 2 provides the methods of the study. It begins by Section 2.1, which introduces the urban physics model. It follows by Section 2.2, which introduces the retrofitted systems considered. It then provides Section 2.3 that describes the economics analysis. It continues with Section 2.4, which provides the greenhouse gas emissions savings analysis. It follows by Section 2.5 that describes the future weather files. In Section 2.6, it describes the micro-genetic optimization algorithm. Section 3 provides the results and discussion. It begins with Section 3.1 to evaluate the base building model against observations of energy consumption. In Section 3.2, the base building electricity and gas consumptions are provided. In Section 3.3 the retrofitted building overall/individual objective functions and GHG emissions savings are discussed. In Section 3.4 the retrofitted building variables are discussed, with their sensitivity to time and future climate scenarios. Finally, the study provides the conclusions in Section 4. A rich set of Appendices in Appendix are provided to demonstrate all the detailed equations and models used by the study. These include the retrofitted building systems and economics models.

2. Methods

2.1. The Urban Physics Model (UPM)

The Vertical City Weather Generator (VCWG) is a computationally-fast Urban Physics Model (UPM) at micro-scale. It calculates the temporal and vertical variation of outdoor urban climate variables, the temporal variation of indoor climate variables, indoor/outdoor surface temperatures, building performance metrics such as space heating/cooling loads, space/water heating loads, domestic electricity use, and natural gas/electricity consumption.

Numerous versions of VCWG have been developed. VCWG v1.3.2 is the original version [30]. It was enabled with renewable and alternative energy integration in VCWG v1.4.5 and v1.4.6 [5]. The main difference between v1.4.5 and v1.4.6 is that v1.4.5 requires use of all renewable and alternative energy features, while v1.4.6 permits utilization of solar photovoltaics and wind energy only, in addition to permitting an overall simulation including solar thermal energy, energy storage, heat pumps, and phase change materials. In this work VCWG v1.4.6 is employed and further developed into VCWG v1.5.0, which includes a micro-genetic optimization feature. VCWG v2.0.0 is another version, which integrates hydrological processes [31] in addition to the original model features of VCWG 1.3.2.

As shown in Fig. 1, VCWG v1.5.0 is comprised of many sub-models: a rural model, a one-dimensional urban vertical diffusion model, a radiation model, a building energy model, and surface energy balance models. VCWG is forced with a weather file from a rural site at the vicinity of the urban area. The rural model predicts the vertical variation of potential temperature, specific humidity, and friction velocity at 10 m a.g.l. The rural model also calculates a horizontal pressure gradient. The rural model outputs are imposed on the urban vertical diffusion model, which computes the vertical transport of potential temperature, momentum, specific humidity, and turbulence kinetic energy. This vertical diffusion model is integrated to the radiation and building energy models utilizing a two-way interaction scheme. The aerodynamic and thermal effects of urban surfaces, surface vegetation, and trees are considered. The feedback interaction coupling scheme among the building energy model, radiation model, and the urban one-dimensional vertical diffusion model is aimed to update the boundary conditions, surface temperatures, and the source/sink terms in the transport equations in successive time step iterations. Table 1 lists the input parameters used for the VCWG simulations [5].

2.2. Retrofitted building systems

This study considers an active thermal energy storage paradigm. Fig. 2 shows the building systems as a combination of Solar Thermal (ST) collector, PhotoVoltaic (PV) collector, Wind Turbine (WT), Building Integrated Thermal Energy Storage (BITES) system, Phase Change Material (PCM), Heat Pump (HP), and heat recovery systems in addition to the use of ground thermal energy. A ground-source HP, which exchanges heat with the building foundation, supplements the conventional space heating (natural gas furnace) and cooling (air conditioning) systems. The BITES is charged and discharged using the ST, HP, exhaust air, supply water, or gray water. The BITES is assumed to be built using concrete, which is commonly used as the foundation structure [22,38]. The BITES system acts as either a cold or warm reservoir of heat for the HP system. A PCM is used to modulate the BITES temperature if BITES temperatures are close to the melting temperature of PCM [39]. Water can be preheated using the BITES

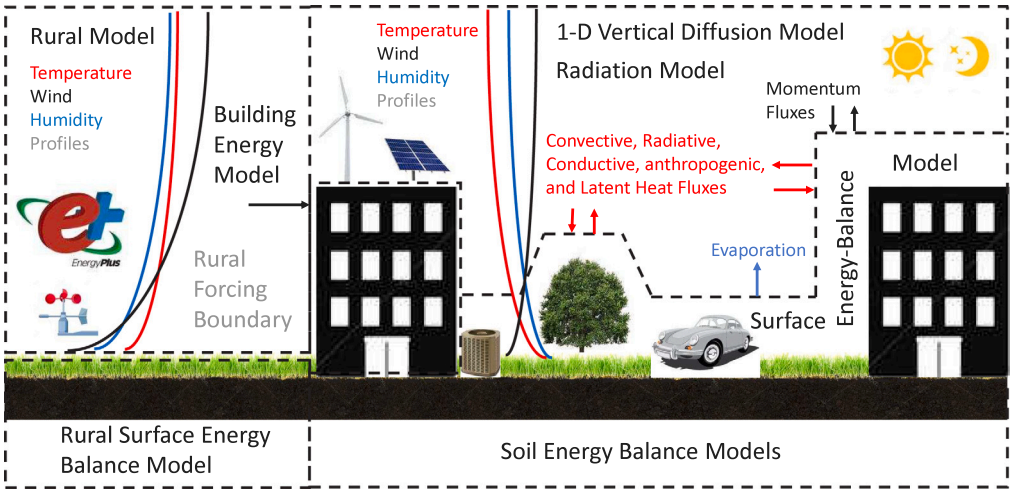

Fig. 1. Illustration of the Vertical City Weather Generator (VCWG v1.5.0) model and the constituent sub-models.

Table 1
List of input parameters used in VCWG v1.5.0 for model exploration in Toronto.

Parameter	Units	Symbol	Toronto
Rural Latitude	[°N]	$\mathrm{lat}_{\mathrm{rur}}$	43.649889
Rural Longitude	[°E]	$\mathrm{lon}_{\mathrm{rur}}$	−80.121909
Urban Latitude	[°N]	lat	43.632580
Urban Longitude	[°E]	lon	−79.581630
Average buildings height	[m]	H_{avg}	6
Width of canyon	[m]	$w_x = w_y = w$	30
Building width to canyon width ratio	[-]	$b_x/w_x = b_y/w_y = b/w$	0.46
Leaf Area Index	[$\mathrm{m^2 m^{-2}}$]	LAI	0.72–1.00
Tree height	[m]	h_t	5
Tree crown radius	[m]	r_t	1.8
Tree distance from wall	[m]	d_t	5
Building type	[-]	–	Mid-rise apartment
Urban albedos (roof, ground, wall, vegetation)	[-]	$\alpha_R, \alpha_G, \alpha_W, \alpha_V$	0.10, 0.13, 0.23, 0.23
Urban emissivities (roof, ground, wall, vegetation)	[-]	$\epsilon_R, \epsilon_G, \epsilon_W, \epsilon_V$	0.95, 0.95, 0.91, 0.96
Ground aerodynamic roughness length	[m]	z_{0G}	0.02
Roof aerodynamic roughness length	[m]	z_{0R}	0.02
Ground vegetation cover fraction	[-]	δ_s	0.5
Rural overall albedo	[-]	α_{rur}	0.14
Rural overall emissivity	[-]	ϵ_{rur}	0.95
Rural aerodynamic roughness length	[m]	$z_{0,\mathrm{rur}} = 0.1 h_{\mathrm{rur}}$	0.2
Rural roughness length for temperature	[m]	$z_{\overline{\Theta},\mathrm{rur}} = 0.1 z_{0,\mathrm{rur}}$	0.02
Rural roughness length for specific humidity	[m]	$z_{\overline{Q},\mathrm{rur}} = 0.1 z_{0,\mathrm{rur}}$	0.02
Rural zero displacement height	[m]	$d_{\mathrm{rur}} = 0.5 h_{\mathrm{rur}}$	1
Rural Bowen ratio	[-]	β_{rur}	0.5
Tree Bowen ratio	[-]	β_{tree}	0.5
Vertical resolution	[m]	Δz	1
Time step	[s]	Δt	60
Canyon axis orientation	[°N]	θ_{can}	0

system if its temperature is greater than the city water temperature to be heated. Ground thermal energy can flow between the deep soil and the BITES system. The model assumes that any electricity produced by the PV or WT systems are net metered to the grid, without requiring electricity storage. The Net Metering Regulation (O. Reg. 541/05) under the Ontario Energy Board Act of 1998 permits met metering for renewable energy up to a capacity of 500 [kW] [40]. Appendix A.1 details the equations that describe the retrofitted systems in VCWG [5].

2.3. Economics analysis

The costs associated with building system retrofits is an important objective function to be reduced. Standard prEN 15459-1 (Economic evaluation procedure for energy systems in buildings) provides the *Global Cost* approach for evaluation of relative economic feasibility of building system configurations [4,41]. In this approach, all expenses/revenues related to building system configurations (such as initial investment, operation and maintenance, fuel/electricity cost, and salvage) are considered. The method accounts for a discounting rate over an investment period of $N = 20$ years. The time value of money can be considered using three alternative cost metrics: (1) present value of the global cost, which evaluates all future costs discounted to the present time; (2) annualized cost, which disperses future costs to an equal annual value, considering the time value of money; and (3) pay-back period, which provides the number of years it takes for the marginal initial cost of a building retrofit configuration to be balanced by the accumulation of revenue from annual fuel/electricity savings [5]. In this study we report the annualized cost as the main economic metric. Appendix A.2 details the equations that describe the economics model in VCWG [5].

2.4. Greenhouse gas emissions savings analysis

The Greenhouse Gas (GHG) emissions savings as a result of retrofitting the building systems can be calculated by quantifying the savings in natural gas and electricity consumptions, compared to the

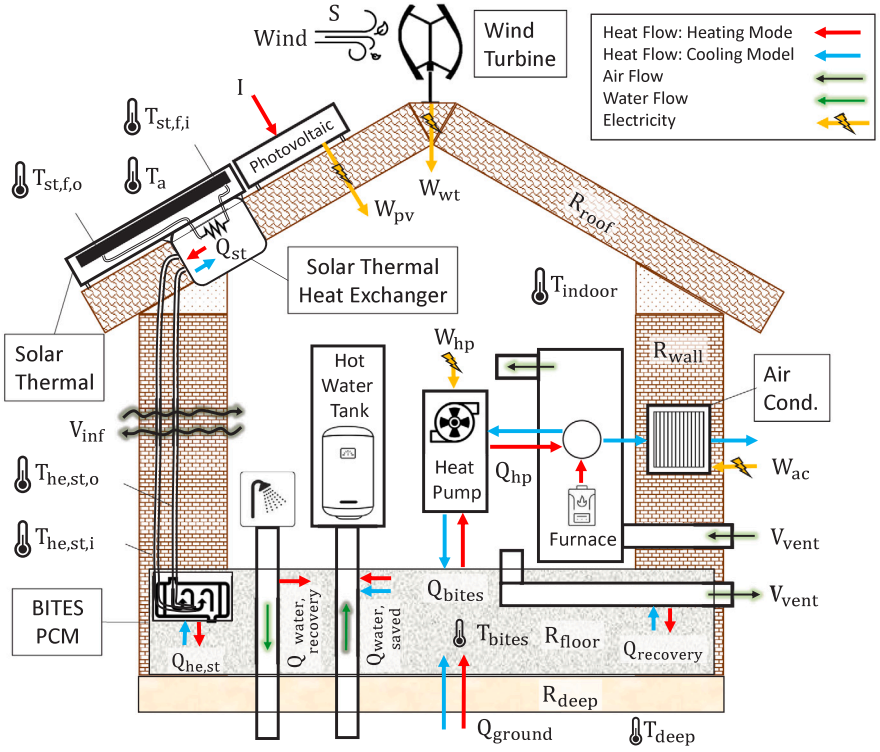

Fig. 2. System configuration to reduce building sensible heating/cooling loads and water heating load via integration of Solar Thermal (ST), PhotoVoltaic (PV), Wind Turbine (WT), Building Integrated Thermal Energy Storage (BITES) system, Phase Change Material (PCM), Heat Pump (HP), and heat recovery systems as well as the utilization of ground thermal energy.

base case. Further, the grid GHG emissions intensity should be factored in the calculation. The savings in natural gas can be calculated using

$$G_{save} = [G_{hB} + G_{whB} - (G_h + G_{wh})]A_{bld}N, \quad (1)$$

where G_{hB} and G_{whB} [m^3m^{-2}] are the natural gas consumption for base case for space and water heating, respectively, and G_h and G_{wh} [m^3m^{-2}] are the natural gas consumption for the retrofitted system for space and water heating, respectively. The savings in GHG emissions, due to savings in natural gas consumption, is

$$GHG_{Gsave} = G_{save}\rho_{CH_4}\frac{MW_{CO_2}}{MW_{CH_4}}, \quad (2)$$

where $\rho_{CH_4} = 0.668$ [$kg - CH_4m^{-3}$] is the density of natural gas (methane), and $MW_{CO_2} = 44$ [$g - CO_2mole^{-1}$] and $MW_{CH_4} = 16$ [$g - CH_4mole^{-1}$] are molecular weights of CO_2 and methane, respectively.

The savings in electricity consumption can be calculated using

$$E_{save} = [E_{cB} + E_{dB} - (E_c + E_h + E_d - E_{pv} - E_{wt})]A_{bld}N, \quad (3)$$

where E_{cB} and E_{dB} [$kW - hrm^{-2}$] are the electricity consumption due to space cooling and domestic use for the base case, E_c, E_h, and E_d [$kW - hrm^{-2}$] are the electricity consumption for the retrofitted system due to space cooling, space heating, and domestic use, respectively, and E_{pv} and E_{wt} [$kW - hrm^{-2}$] are electricity produced using the PV and WT, respectively. The savings in GHG emissions, due to savings in electricity consumption, is

$$GHG_{Esave} = E_{save}EI_E, \quad (4)$$

where $EI_E = 0.04$ [$kg - CO_2kW - hr^{-1}$] is the grid electricity emissions factor in Ontario.

2.5. Future climate weather files

The Vatic Weather File Generator (VWFG) is a computationally-fast statistical downscaling model to generate future weather files for building simulations [42]. This approach is based on the morphing technique, where the statistics of future weather variables (e.g. mean and standard deviation) are matched with historical weather files [43]. The statistical downscaling model uses data from three time periods to generate future weather files: the historical time period (1980–1999), the validation time period (2007–2020), and the future time period (2021–2100). The historical and validation weather files are retrieved from ERA5 reanalysis products [44]. The format for the weather files is the EnergyPlus Weather (EPW). The historical, validation, and future Climate Model (CM) records are retrieved from the CanRCM4 regional climate model. CanRCM4 is Canada's primary and current regional climate model [45]. It is known to exhibit warm (temperature) and wet (precipitation) biases [46]. VWFG removes the biases for temperature, wind, pressure, and radiation fluxes within CanRCM4 using statistical corrections [42]. VWFG (1) applies a bias correction process to the validation/future weather variables to improve the accuracy of the downscaling method [47]; (2) considers weighting of key weather variables to match validation/future and historical weather conditions [48–50]; and (3) corrects the monthly mean and standard deviation of validation/future weather variables given the mean and standard deviation of weather variables in the regional climate model [43]. The climate of Toronto, Canada, is analyzed for two Representative Concentration Pathway (RCP) scenarios of 4.5 and 8.5 [Wm^{-2}].

2.6. Micro-genetic optimization

The micro-genetic optimization method is applied from Park and Park [12]. Most common genetic optimization algorithms use large populations up to 100 and apply cross-over, mutation, crowding, and other probabilistic processes to create new generations [3]. However, the micro-genetic optimization method uses a small population size (about 5), applies the cross-over/mutation processes, and updates the population via inner loop iterations (using offsprings to make the next

Table 2
Optimization variables with minimum value, maximum value, and variation interval.

Symbol	Units	Description	Minimum	Maximum	Interval
V_{bites}	[m^3m^{-2}]	Volume of BITES	0.01	0.20	0.01
α_R	[-]	Roof Albedo	0.1	0.7	0.05
$\dot{m}_{st,f}$	[$kgs^{-1}m^{-2}$]	Working Fluid Flow Rate for ST	0.0001	0.002	0.0001
A_{st}	[m^2m^{-2}]	Collector Area for ST	0.2	0.6	0.05
R_{roof}	[m^2KW^{-1}]	Roof Thermal Resistance	5.5[a]	8	0.5
V_{pcm}	[m^3m^{-2}]	Volume of PCM	0.01	0.20	0.01
V_{inf}	[ACH]	Infiltration Rate	0.5	3.5[a]	0.5
R_{wall}	[m^2KW^{-1}]	Wall Thermal Resistance	3.5[a]	7.5	0.5
V_{vent}	[$Ls^{-1}m^{-2}$]	Ventilation Rate	0.3[a]	0.6	0.05
GR	[-]	Glazing Ratio	0.1	0.5[a]	0.05
$\dot{m}_{he,st}$	[$kgs^{-1}m^{-2}$]	Air Flow Rate for ST	0.001	0.02	0.001
T_{melt}	[K]	Melting Temperature of PCM	290	310	2
A_{wt}	[m^2m^{-2}]	Swept Area of WT	0.05	0.2	0.05
$SHGC$	[-]	Solar Heat Gain Coefficient ($SHGC$)	0.1	0.7[a]	0.1
A_{pv}	[m^2m^{-2}]	Collector Area for PV	0.1	0.6	0.1

[a]Base building configuration.

generation) and outer loop iterations (re-sampling the search space to make the next generation).

Table 2 shows the variable space for optimization. For each of the 15 variables, the minimum value, maximum value, and variation interval is specified. The typical two-storey residential house in Toronto is characterized using Natural Resources Canada's definition for its equivalent Energy Use Intensity (EUI) being greater than 225 [$ekW-hrm^{-2}year^{-1}$] [33]. Such a house is characterized by codes and standards for envelop thermal resistance (roof, wall, and window), infiltration rate, ventilation rate, glazing ratio, Solar Heat Gain Coefficient ($SHGC$), thermal efficiency of its heating devices (furnace and hot water heater), and Coefficient of Performance (COP) for its air conditioning. Except for thermal efficiency and COP, the other building system variables mentioned above are optimized in this study. Other variables are optimized that are related to renewable energy systems such as solar thermal energy, electricity generated using photovoltaic panels, and electricity generated using wind turbines. In addition, other variables are optimized that are related to alternative energy systems such as building integrated thermal energy storage and phase change materials. The code/standard compliant variables are listed in Table 2 as either the minimum (for thermal resistance and ventilation) or maximum (for infiltration, $SHGC$, and glazing ratio) values for each range.

Various building standards have been used to set the ranges for the optimization variables. These standards include NECB [51], ASHRAE 62.1 [52], ASHRAE 62.2 [53], ASHRAE 90.1 [54], and ASHRAE 90.2 [55].

Regarding thermal storage of heat, the BITES system is assumed to be constructed with concrete, which is part of the pre-existing foundation of the residential building. The PCM is assumed to be made of inorganic salt hydrates, which have melting temperatures close to ambient conditions. However, it is non-trivial what quantity and at what melting temperature the PCM characteristics will be optimum.

Regarding the envelop thermal properties, the roof albedo is set to a wide range of values since the optimum value is not trivial. It is not known *a priori* which albedo will result in overall energy savings for the Canadian climate. On the one hand, high albedos are desirable in the Summer season to reduce the building cooling load. On the other hand, low albedos may be desired in the Winter season to reduce the building heating load. The roof thermal resistance is determined using Table 5.5-5 in ASHRAE 90.1 [54] and Table 3.2.2.2 in NECB [51]. The wall thermal resistance is determined using Table 5.5-5 in ASHRAE 90.1 [54] and Table 3.2.2.2 in NECB [51].

Regarding the use of renewable energy, the optimization method shall determine the optimum value of ST collector area, PV collector area, and WT swept area. Further, the mass flow rate of the working fluid in ST is not trivial. High mass flow rates will result in large amounts of heat collection from the ST system, but at the expense of lower temperatures; on the other hand, low mass flow rates will result in harnessing solar thermal energy at higher temperatures, but at the expense of lower heat quantities. A similar argument can be put forth for the mass flow rate of air in the ST heat exchanger, which governs the temperature and the rate, at which solar thermal energy is transferred to the BITES system.

Regarding indoor/outdoor air exchange, the infiltration rate is inferred via Sentence C3.5.5.3 in ASHRAE 90.1 [54] and Sentence 6.3.2 in ASHRAE 90.2 [55]. The ventilation rate is determined from Table 6.1 in ASHRAE 62.1 [52] and Table 4-1b in ASHRAE 62.2 [53].

Regarding windows' configuration, the Glazing Ratio is inferred from Table 5.5-5 in ASHRAE 90.1 [54] and Table A-3.2.1.4(1) in NECB [51]. The Solar Heat Gain Coefficient ($SHGC$) is determined using Table 5.5-5 in ASHRAE 90.1 [54], Table 6-2 in ASHRAE 90.2 [55], and Table 3.2.2.3 in NECB [51]

Fig. 3 shows the schematic for the algorithm of the micro-genetic optimization method, and Fig. 4 shows the schemes used to create a new population. The algorithm consists of two loops: the inner and outer loops. The inner loop uses the same parent population with building variables (genes) to create new offsprings, while the outer loop samples new parents using a uniform random generator for each building variable (gene). At the end of each iteration, the total gas consumption G [m^3m^{-2}] and total electricity consumption E [$kW-hrm^{-2}$] are computed via

$$G = G_h + G_{wh}, \tag{5}$$

$$E = E_h + E_c + E_d - E_{pv} - E_{wt}, \tag{6}$$

where G_h and G_{wh} [m^3m^{-2}] are gas consumption for space and water heating, respectively, E_h, E_c, and E_d [$kW-hrm^{-2}$] are electricity consumption for space heating, space cooling, and domestic use, respectively, and E_{pv} and E_{wt} [$kW-hrm^{-2}$] are electricity generated using PV and WT, respectively.

At the end of each iteration, a fitness function is computed for each individual in the population by a weighted sum of three objective functions. This function is calculated by normalizing and equal-weighting of total gas consumption G [m^3m^{-2}], total electricity consumption E [$kW-hrm^{-2}$], and marginal annualized cost C [$] [8]

$$F = w_G\frac{G}{G_0} + w_E\frac{E}{E_0} + w_C\frac{C}{C_0} \tag{7}$$

where $w_G = w_E = w_C = \frac{1}{3}$ in this study and G_0 [m^3m^{-2}], E_0 [$kW-hrm^{-2}$], and C_0 [$] are normalizing values taken as the solution of the first iteration of the optimization process. The normalization is necessary to avoid letting the objective function with the highest relative value in scale to dominate the other objective functions. Certainly, the weights can be changed if more emphasis shall be placed on reducing an objective function. For instance $w_G = 0.2$, $w_E = 0.2$, and $w_C = 0.6$ will emphasize on minimizing the marginal annualized

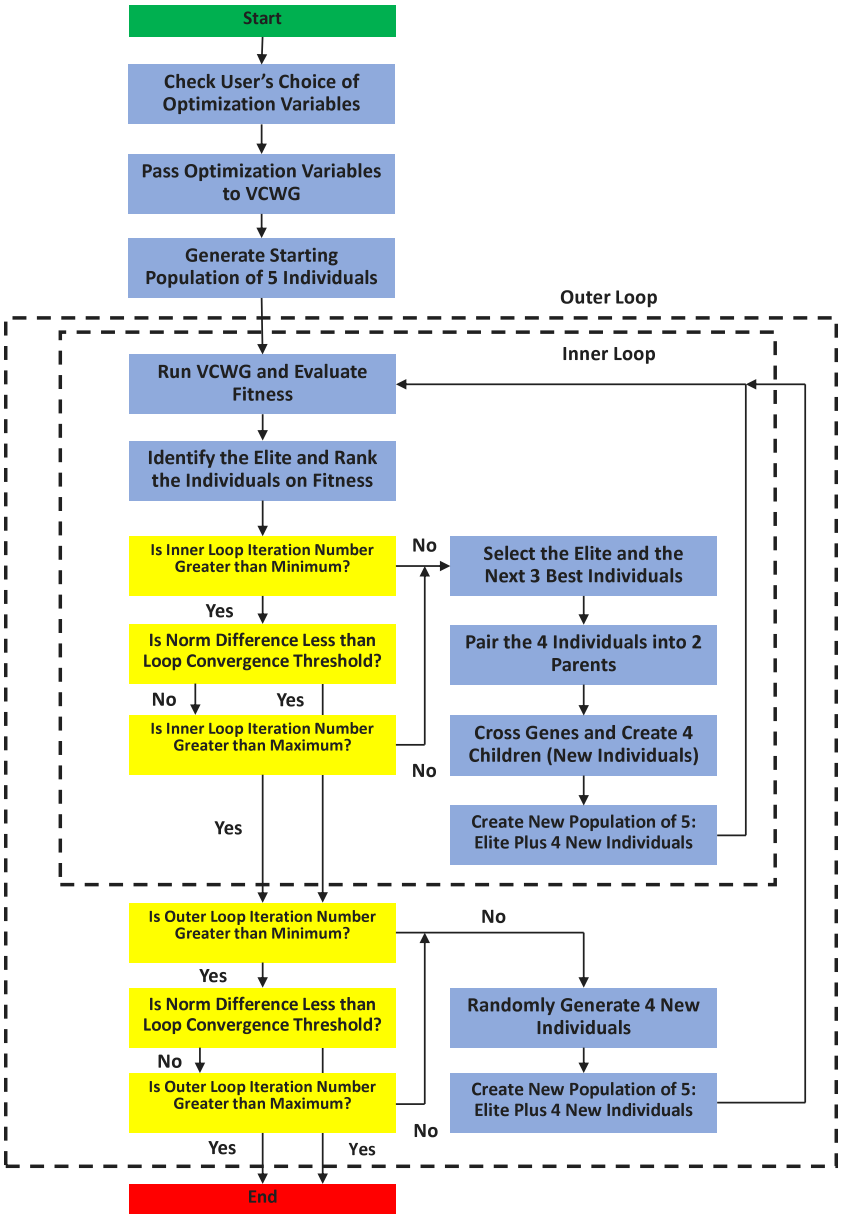

Fig. 3. The algorithm for the micro-genetic optimization method.

cost, rather than minimizing total gas and electricity consumptions. It must be noted the GHG emissions saving is not explicitly considered as an objective function. However, the combination of gas and electricity consumption, implicitly, consider the GHG emissions saving. In other words, reducing both gas and electricity consumption is equivalent to GHG emissions savings.

As shown in Fig. 4, the elite individual is the individual with the lowest fitness function. This individual is preserved for the subsequent population, regardless of whether the inner or outer loops are executed. The individual with the highest fitness function will be discarded. As shown in the figure, when the inner loop is executed, the elite plus three surviving individuals form two sets of parents. Their genes are crossed at an arbitrary point to create four new offsprings, which form the population for the next iteration. When the outer loop is executed, the elite is kept, while four new individuals are randomly sampled to create a new population for the next iteration.

The inner and outer loops are controlled by six loop variables. There are minimum ($I_{min,inner} = 2$) and maximum ($I_{max,inner} = 6$) number of iterations for the inner loop. There are minimum ($I_{min,outer} = 10$) and maximum ($I_{max,outer} = 12$) number of iterations for the outer loop. Further, to check for convergence in each loop, the norm difference between the two successive lowest fitnesses are computed. These fitness values are associated with the elite individual for the two successive iterations, for either the inner or outer loops. The norm difference for fitness F is given by

$$N_F = \frac{|F^n - F^{n-1}|}{F^{n-1}} \tag{8}$$

where $n-1$ and n refer to two successive iteration numbers. The convergence threshold for the norm difference is $N_{F,t,inner} = 0.03$ for the inner loop and $N_{F,t,outer} = 0.001$ for the outer loop. The six loop control variables are determined by trial and error. In a sensitivity study (now shown), we found that for each case a sample of 3 runs, with a total number of optimization iterations of about 30, result in mean individual objective functions (gas consumption, electricity consumption, and cost) that do not change more than 5 [%] in successive iterations. Even though convergence cannot be established formally for population-based stochastic optimization algorithms, this provide evidence that 3 runs and an overall number of optimization iterations

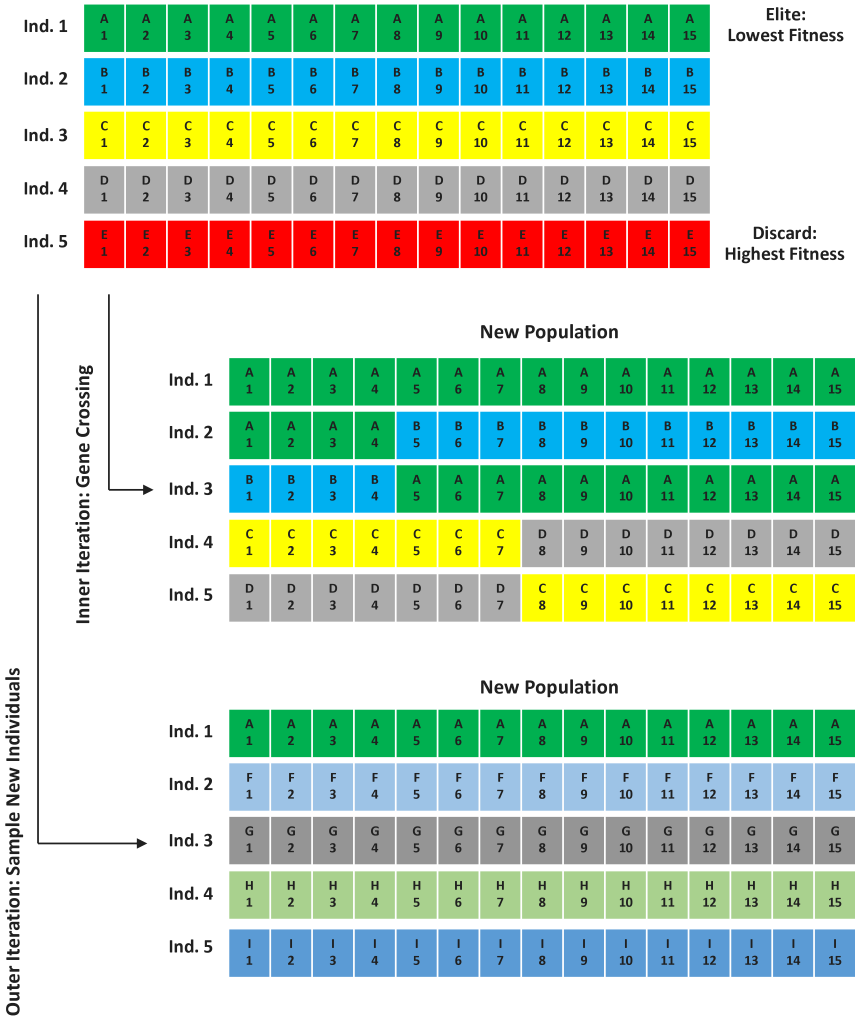

Fig. 4. The schemes used to create a new population for the micro-genetic optimization algorithm: inner iteration with gene crossing and outer iteration with sampling new individuals for the population.

Table 3
Micro-gnetic optimization algorithm control variables.

Symbol	Definition	Value
w_G	Objective function weighing factor for gas consumption	1/3
w_E	Objective function weighing factor for electricity consumption	1/3
w_C	Objective function weighing factor for marginal annualized cost	1/3
$I_{min,inner}$	Minimum inner iterations	2
$I_{max,inner}$	Maximum inner iterations	6
$I_{min,outer}$	Minimum outer iterations	10
$I_{max,outer}$	Maximum outer iterations	12
$N_{F,t,inner}$	Convergence threshold for inner loop	0.03
$N_{F,t,outer}$	Convergence threshold for outer loop	0.001

beyond 30 result in a nearly global optimized solution. These conditions are met given the algorithm control variable settings. Table 3 shows the control variables for the micro-genetic optimization algorithm.

3. Results and discussion

3.1. Evaluation of the base building model

ASHRAE Standard 140 offers a comprehensive method of test for the evaluation of building energy analysis computer programs [56]. The standard develops three philosophies of testing: (1) empirical validation, (2) analytical verification, and (3) comparative modeling. Many building variables can be targeted for such evaluation, such as annual heating/cooling loads, peak heating/cooling loads, minimum/maximum indoor temperature, and gas/electricity consumption [57]. For our study the building energy metrics involving consumption/generation of electricity and consumption of gas are paramount, as they relate to the operational GHG emissions of the building. In fact, ASHRAE Guideline 14 targets the modeling of building energy metrics, and it considers a model calibrated if it can predict the energy metrics of a building within ±5 [%] of the observations [58]. The building energy model within VCWG has been tested empirically against many observations.

Bueno Unzeta [59] compared daily-average building consumption of electricity and gas as they were predicted using the Urban Weather Generator (UWG) software against observations in Toulouse (France) for a mid-rise apartment in 2005. He found good agreement between the model and the observations. The original building energy model within UWG is the same as the model within VCWG.

To validate VCWG predictions of gas and electricity consumption against metered data, a survey program has begun by the authors. Single-detached residential house owners in the Greater Toronto Area (GTA) are asked to provide information about their monthly energy bills (gas and electricity) for a minimum of 1 year. Seven houses have participated in this survey so far, and, for each house, up to 3 years of monthly data are provided in 2020, 2021, and 2022. Corresponding

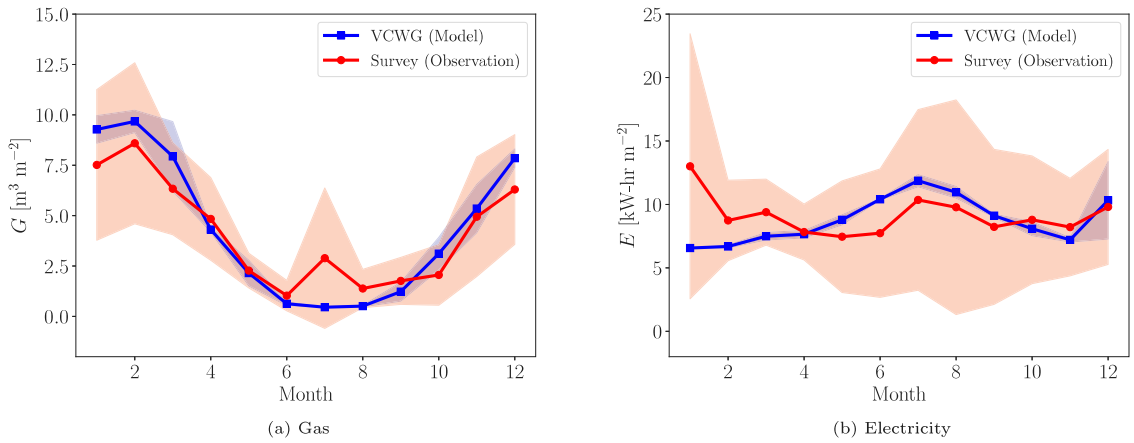

Fig. 5. Monthly consumption of gas [m^3m^{-2}] and electricity [$kW-hrm^{-2}$] per building footprint area as predicted by VCWG and 7 metered single-detached residential houses in the Greater Toronto Area (GTA) in 2020, 2021, and 2022; the main legend shows the mean monthly consumption; the pale blue (VCWG) and red (Survey) regions show 1 standard deviation of the consumption for either the model or observations, respectively; (a) Gas and (b) Electricity. (For interpretation of the references to color in this figure legend, the reader is referred to the web version of this article.)

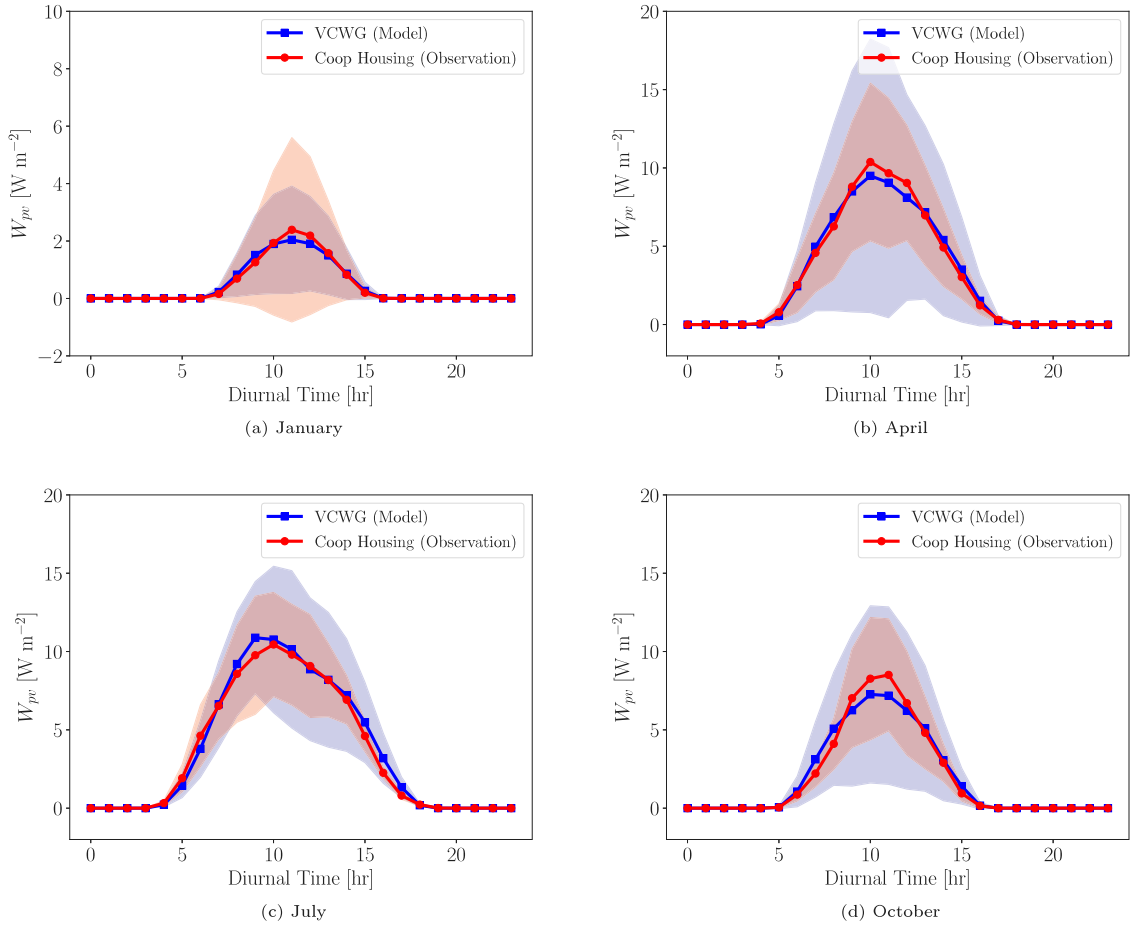

Fig. 6. Mean diurnal variation of hourly PV power [Wm^{-2}] per building footprint area as predicted by VCWG and measured at the Coop Housing building (University of Guelph); simulations are conducted for 2022; the main legend shows the mean hourly PV power for a duration of a month; the pale blue (VCWG) and red (Coop Housing) regions show 1 standard deviation of the PV power for either the model or observations, respectively; (a) January, (b) April, (c) July, and (d) October. (For interpretation of the references to color in this figure legend, the reader is referred to the web version of this article.)

VCWG simulations have been run for a typical single-detached house introduced in Section 2.6 as the base building (without retrofits) for the same three years. The base building does not feature any of the alternative or renewable energy systems (PV, WT, HP, BITES, PCM, and energy recovery). Fig. 5 shows the comparison. The relative errors in the mean annual gas and electricity consumptions are 5.2 [%] and −3.8 [%], respectively. The authors particularly noted that some houses use more electricity in the winter (possibly due to auxiliary electrical heating), while other houses use more electricity in the summer (possibly due to air conditioning).

We further tested the limited aspect of renewable electricity generation by the PV system as predicted by VCWG and compared it to

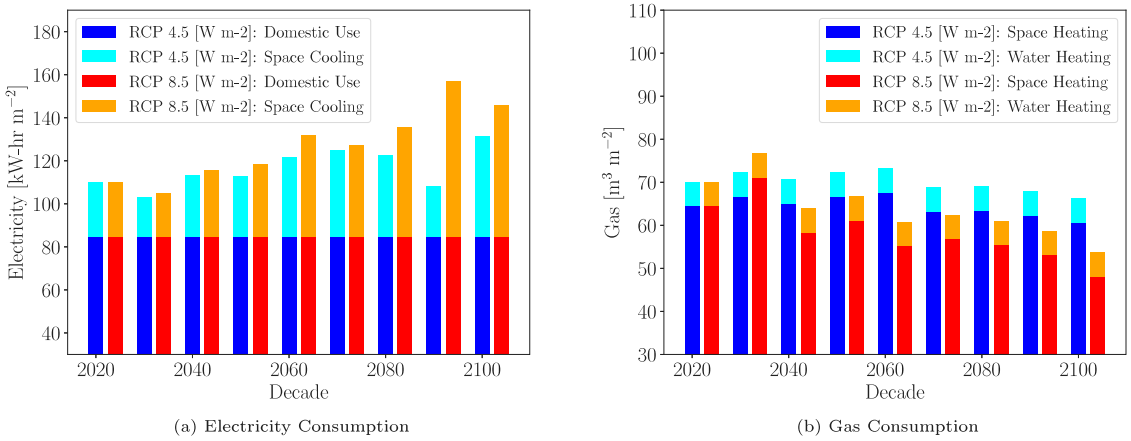

Fig. 7. Base building energy consumption under two RCP scenarios of 4.5 and 8.5 [Wm^{-2}]; (a) electricity consumption and (b) gas consumption.

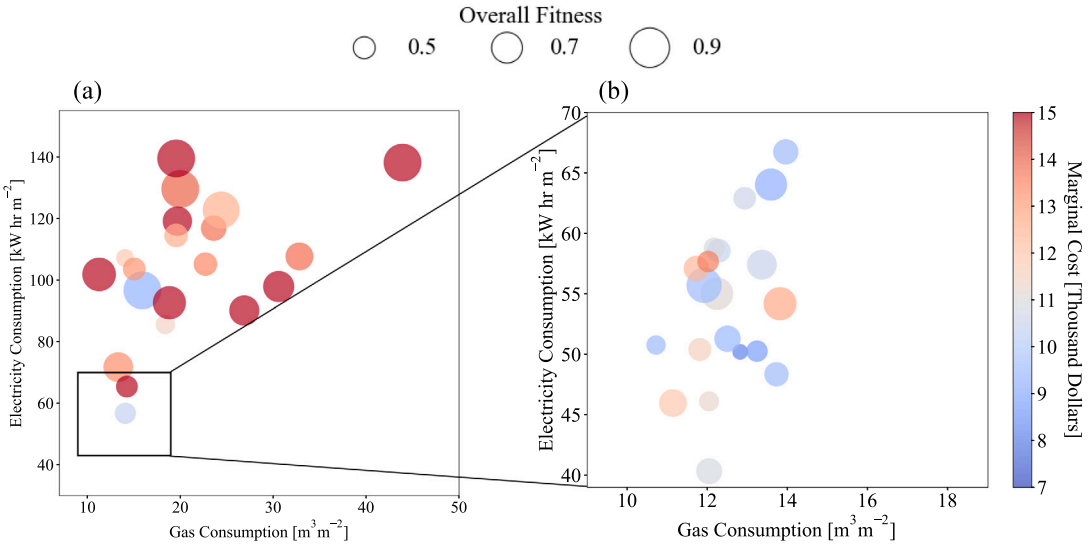

Fig. 8. Cluster map of objective functions for a single run of the optimization algorithm for the retrofitted building in 2020; (a) overall range for the objective functions (b) zoomed-in range for the objective functions.

the actual observations for a small office (Coop Housing building at the University of Guelph). This building was simulated using VCWG for the entire year of 2022. Fig. 6 shows the comparison for selected months. VCWG predicted the mean daily PV power within 2 [%] of the observations.

3.2. Base building electricity and gas consumption

From 2020 to 2100, it is expected that the dry bulb temperature for Toronto, on annual average, will increase by 0.027 and 0.062 [Kyear^{-1}] for RCPs 4.5 and 8.5 [Wm^{-2}], respectively [42]. We expect greater electricity consumption for space cooling (air conditioning) and less gas consumption for space heating under both RCP scenarios. Further, we expect that the changes in electricity and gas consumption be more accentuated under RCP 8.5 [Wm^{-2}]. Fig. 7 shows the electricity and gas consumption for a base building (without retrofits), for every decade from 2020 until 2100 using one representative year for each decade (i.e. for years 2020, 2030, 2040, etc.). The electricity consumption is divided into domestic use and space cooling, while the gas consumption is divided into water heating and space heating. The figure shows the expected trends in the energy consumption noted above. Regarding electricity consumption, all of the change is associated with the need for space cooling. Regarding the gas consumption, almost all of the change is associate space heating. Note that the water heating demand is a function of deep soil temperature, which is not predicted to change as drastically as atmospheric temperatures (not shown).

3.3. Retrofitted building overall/individual objective functions and GHG emissions savings

Figs. 8 and 9 show the cluster map of individual objective functions and the individual/overall objective functions versus optimization iteration, respectively, throughout the optimization process for year 2020. The initial solution for the retrofitted building is randomly sampled from the variables space noted in Table 2. Given the random choice of such variables, the optimization is repeated for 3 runs. In Fig. 9 the left panel shows the result for only 1 run, while the right panel shows the results for the 3 runs.

From Figs. 8 and 9(a) it can be noted that the micro-genetic algorithm reduces the individual objective functions substantially within only 30–40 overall iterations. The process indicates that all three objective functions of cost, gas consumption, and electricity consumption can be reduced simultaneously. This is attractive compared to particle swarm and ant colony methods, which require many hundreds of iterations to substantially reduce the objective functions. Further, such

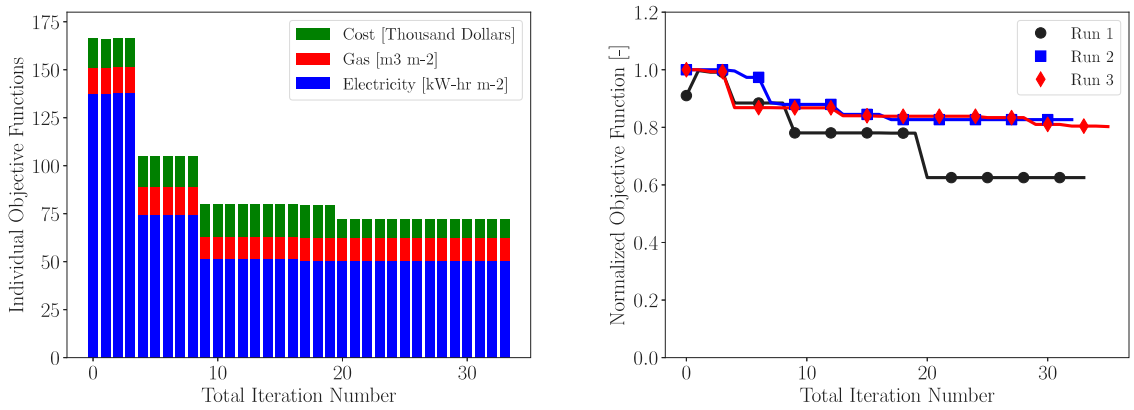

(a) Individual Objective Functions (b) Overall Objective Function

Fig. 9. Objective functions versus optimization iteration for the retrofitted building in 2020; (a) individual objective functions for a single run (1) and (b) overall normalized objective function for 3 runs (1, 2, 3); symbols show the onset of outer loop iterations.

Table 4
Average electricity consumption and savings for the base and retrofitted buildings.

Year	Base building [kW – hrm^{-2}]	Retrofitted building [kW – hrm^{-2}]	Savings [%]	Base building [kW – hrm^{-2}]	Retrofitted building [kW – hrm^{-2}]	Savings [%]
	RCP 4.5 [Wm^{-2}]			RCP 8.5 [Wm^{-2}]		
2020	110.00	56.38	48.74	110.00	56.38	48.74
2030	103.00	56.93	44.73	105.00	60.13	42.73
2040	113.00	66.75	40.93	115.00	68.54	40.40
2050	113.00	66.36	41.27	118.00	60.26	48.93
2060	121.00	72.83	39.81	132.00	50.54	61.71
2070	125.00	59.15	52.68	127.00	68.18	46.31
2080	122.00	64.82	46.87	135.00	75.41	44.14
2090	108.00	61.81	42.77	157.00	65.65	58.18
2100	131.00	67.51	48.47	146.00	67.01	54.10

Table 5
Average gas consumption and savings for the base and retrofitted buildings.

Year	Base building [m^{3}m^{-2}]	Retrofitted building [m^{3}m^{-2}]	Savings [%]	Base building [m^{3}m^{-2}]	Retrofitted building [m^{3}m^{-2}]	Savings [%]
	RCP 4.5 [Wm^{-2}]			RCP 8.5 [Wm^{-2}]		
2020	69.90	12.65	81.90	69.90	12.65	81.90
2030	72.20	14.38	80.08	76.60	13.28	82.67
2040	70.70	13.52	80.88	63.80	11.91	81.33
2050	72.40	13.37	81.53	66.60	11.71	82.42
2060	73.40	12.50	82.97	60.90	11.22	81.57
2070	68.80	12.73	81.50	62.50	11.20	82.09
2080	69.00	12.46	81.94	61.10	11.90	80.53
2090	67.90	13.77	79.72	58.60	11.50	80.37
2100	66.00	12.36	81.27	53.80	10.65	80.20

methods require a large population of solutions, which is computationally beyond the capacity of VCWG [9,10]. Another attractive feature of the micro-genetic algorithm is that it attempts to find a global minimum every time the population is randomly re-sampled for the outer loop.

From Fig. 9(b) it can be seen that the 3 solutions (3 runs) do not reach the same final normalized overall objective function. Two overall objective functions are reduced by about 10 [%], while the third overall objective function is reduced by about 40 [%]. This is due to the fact that the initial solution is randomly chosen and used for normalization of the subsequent solutions at later iterations. This random feature is common in all the subsequent results. The following analysis uses 3 runs to investigate the optimum solution under different future climate change scenarios. To account for the solution variability, the average and standard deviation of the solutions over the 3 runs are reported.

Fig. 10 shows the energy consumption of base and retrofitted buildings. As expected for the base building without retrofitted systems, with climate warming, the electricity consumption increases, due to increasing cooling demand, and the gas consumption decreases, due to decreasing heating demand, from 2020 to 2100. For the retrofitted case, the average (line) and 1 standard deviation (shaded band) over 3 runs are shown. The retrofitted building offers great opportunity for energy savings.

Tables 4 and 5 quantify the average electricity and gas consumptions and savings for the base and retrofitted buildings. The electricity savings are within 39.81–52.68 [%] and 40.40–61.71 [%] for RCPs 4.5 and 8.5 [Wm^{-2}], respectively. Given future climate projections, the cooling demand or potential electricity savings of buildings do not change monotonically over the decades; rather some decades may experience greater cooling demand or potential electricity savings than others. This is due to the projected climate conditions, particularly the ambient temperature [42]. The gas savings are within 79.72–82.94 [%] and 80.20–82.67 [%] for RCPs 4.5 and 8.5 [Wm^{-2}], respectively. It appears that electricity savings are more variable from one decade to the next than the gas savings. This may relate to occurrence of

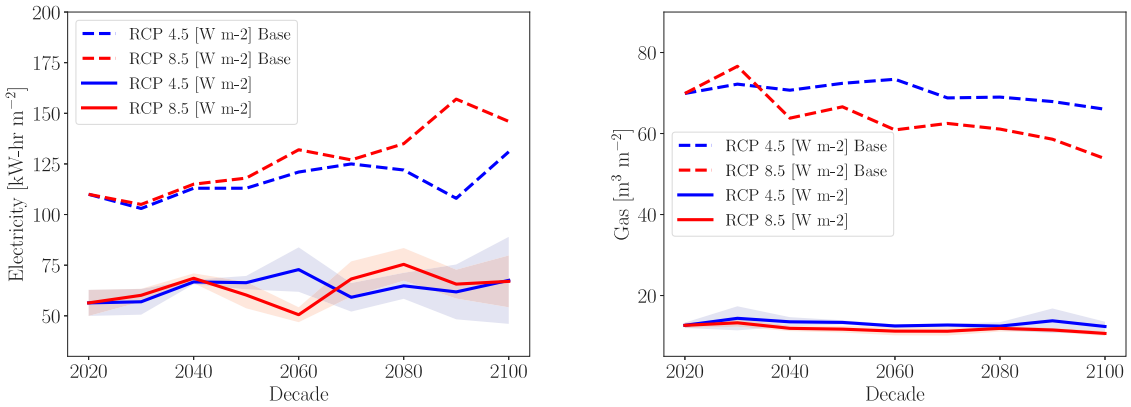

Fig. 10. Energy consumption of base and retrofitted buildings from 2020 to 2100 under two RCP scenarios of 4.5 and 8.5 [Wm^{-2}]; (a) electricity consumption and (b) gas consumption; for the retrofitted case, the average (line) and 1 standard deviation (shaded band) over 3 runs are shown.

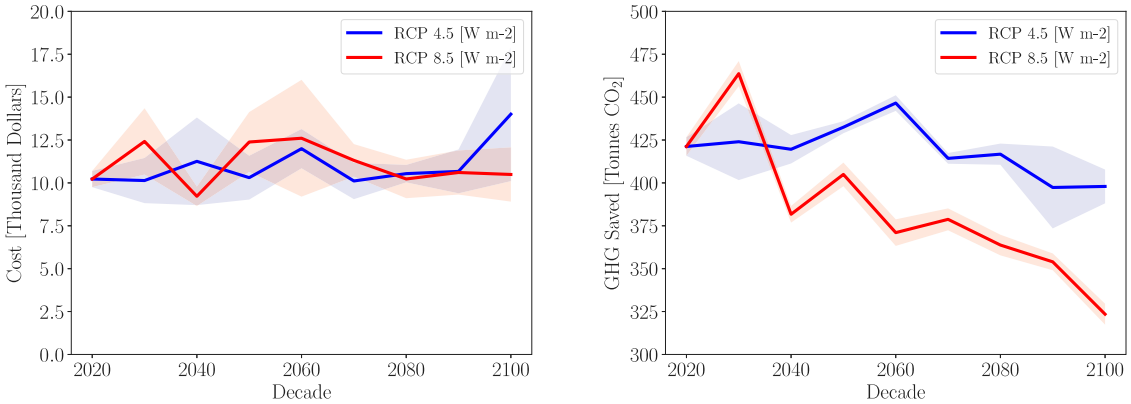

Fig. 11. The annualized retrofit cost and GHG emissions saving over 20 years from 2020 to 2100 under two RCP scenarios of 4.5 and 8.5 [Wm^{-2}]; (a) cost and (b) GHG emissions savings; for the retrofitted case, the average (line) and 1 standard deviation (shaded band) over 3 runs are shown.

short-lived heat waves that can unpredictably demand excessive air conditioning from one decade to the next; rather than base line heating demands with lesser variability from one decade to the next.

Fig. 11 shows the annualized retrofit cost and the GHG emissions savings over 20 years. The annualized retrofit cost, about 10–15 thousand Dollars, is not affected substantially by the decades and the future climate change scenario. This cost can be interpreted as the *green premium*, i.e. the price a home owner shall pay to reduce their GHG emissions. The retrofitted systems will save large amounts of GHG emissions in the range 325–475 [TonnesCO_2] over the duration of 20 years. The GHG emissions savings decline from 2020 to 2100, and the savings potential is substantially reduced for the RCP 8.5 compared to the RCP 4.5 [Wm^{-2}] climate change scenario. We suggest that with the more extreme climate change scenario of RCP 8.5 [Wm^{-2}], the building energy needs in the future will be enhanced, particularly the cooling demand, so that modest and cost-effective retrofits considered in this study cannot result in GHG emissions savings for the distant future as effectively as the earlier decades.

3.4. Retrofitted building variables

Tables 6 and 7 show the trends for the average of optimized solutions from 2020 to 2100 under the two RCP 4.5 and 8.5 [Wm^{-2}] scenarios. One key question is whether some optimized variables will not be affected by climate change scenario in the future. In other words, are there optimum solutions regardless of future climate change? Another key questions is whether some optimized variables will be affected by climate change scenario in the future. To answer this question, either decade by decade variations of the optimized solutions can be analyzed, or trend lines can be fitted to the optimized solution, and percent change of the optimized solution per decade can be computed using the slope of the trend lines to find the change over the entire time horizon of 2020 to 2100 [60]. We will first discuss the optimized solutions that do now show sensitivity to climate change scenarios in the future. We will then discuss the optimized solutions that show such sensitivity.

From Tables 6 and 7 we note that the optimized thermal resistance of roof R_{roof} [m^{2}KW^{-1}] is closer to the middle of the permissible range, 5.5–8 [m^{2}KW^{-1}], and the optimized thermal resistance of wall R_{wall} [m^{2}KW^{-1}] is also closer to the middle of the permissible range, 3.5–7.5 [m^{2}KW^{-1}]. The optimum values are confounded by the combined effects of heat gain/loss throughout the cooling/heating/shoulder seasons. The optimized infiltration rate V_{inf} [ACH], however, is closer to the minimum of the permissible range, 0.5 [ACH], and the optimized ventilation rate V_{vent} [Ls^{-1}m^{-2}] is also closer to the minimum of the permissible range, 0.3–0.6 [Ls^{-1}m^{-2}], suggesting that fresh air exchange with the outdoor environment generally results in greater energy consumption for cooling and heating. It must be noted that such minimum air exchange rates are vital from the point of view of indoor air quality, and they cannot be eliminated [61]. The optimized Glazing Ratio GR [-] is also found to be closer to the minimum of the permissible range, 0.1–0.5 [-], suggesting that unwanted heat transfer through windows generally results in greater building energy consumption. The minimum glazing ratio should be maintained from the perspective of indoor health. The optimized collector area for PV

Table 6
Time trend of the average optimized variables for RCP 4.5 [Wm^{-2}]; the percent change is calculated over one decade.

Symbol	Units	2020	2030	2040	2050	2060	2070	2080	2090	2100	% Change
V_{bites}	[m^3m^{-2}]	0.0533	0.0333	0.0167	0.0533	0.0300	0.0367	0.0133	0.0833	0.0667	6.98
α_R	[-]	0.233	0.550	0.517	0.467	0.500	0.367	0.417	0.283	0.267	−4.03
$\dot{m}_{st,f}$	[$gs^{-1}m^{-2}$]	0.333	0.533	0.433	0.867	0.867	0.633	0.867	0.900	0.600	6.96
A_{st}	[m^2m^{-2}]	0.333	0.467	0.383	0.467	0.367	0.433	0.583	0.217	0.350	−1.32
R_{roof}	[m^2KW^{-1}]	6.83	6.00	7.33	6.83	6.00	6.33	6.50	7.17	7.67	1.15
V_{pcm}	[m^3m^{-2}]	0.0233	0.0233	0.0467	0.0300	0.0633	0.0200	0.0300	0.0267	0.0833	8.94
V_{inf}	[ACH]	0.500	0.500	0.500	0.500	0.500	0.500	0.500	0.667	0.500	1.61
R_{wall}	[m^2KW^{-1}]	5.17	4.83	4.50	5.00	5.33	5.50	6.17	4.33	5.50	1.19
V_{vent}	[$Ls^{-1}m^{-2}$]	0.467	0.383	0.433	0.350	0.300	0.367	0.350	0.333	0.383	−2.82
GR	[-]	0.133	0.250	0.150	0.183	0.167	0.167	0.100	0.217	0.183	−0.16
$\dot{m}_{he,st}$	[$kgs^{-1}m^{-2}$]	0.0070	0.0147	0.0083	0.0107	0.0103	0.0090	0.0063	0.0067	0.0093	−3.70
T_{melt}	[K]	305	300	305	296	299	300	299	298	301	−0.15
A_{wt}	[m^2m^{-2}]	0.117	0.117	0.083	0.083	0.083	0.117	0.117	0.117	0.133	2.59
$SHGC$	[-]	0.533	0.300	0.367	0.367	0.433	0.367	0.467	0.367	0.300	−2.29
A_{pv}	[m^2m^{-2}]	0.600	0.600	0.600	0.567	0.533	0.600	0.533	0.600	0.567	−0.67

Table 7
Time trend of the averaged optimizated variables for RCP 8.5 [Wm^{-2}]; the percent change is calculated over one decade.

Symbol	Units	2020	2030	2040	2050	2060	2070	2080	2090	2100	% Change
V_{bites}	[m^3m^{-2}]	0.0533	0.0867	0.0233	0.0300	0.0400	0.0767	0.0333	0.0400	0.0567	−2.05
α_R	[-]	0.233	0.417	0.417	0.467	0.400	0.383	0.350	0.483	0.300	1.09
$\dot{m}_{st,f}$	[$gs^{-1}m^{-2}$]	0.333	0.267	0.467	0.733	0.800	0.867	0.433	1.033	1.233	14.51
A_{st}	[m^2m^{-2}]	0.333	0.367	0.467	0.383	0.367	0.400	0.317	0.450	0.567	3.70
R_{roof}	[m^2KW^{-1}]	6.83	6.17	6.67	6.17	6.83	7.33	6.17	6.83	6.50	0.21
V_{pcm}	[m^3m^{-2}]	0.0233	0.0667	0.0167	0.0667	0.0767	0.0333	0.0233	0.0300	0.0300	−4.23
V_{inf}	[ACH]	0.500	0.500	0.500	0.500	0.500	0.500	0.500	0.500	0.500	0.00
R_{wall}	[m^2KW^{-1}]	5.17	5.17	5.00	5.83	6.67	5.50	4.17	5.00	5.17	−0.79
V_{vent}	[$Ls^{-1}m^{-2}$]	0.467	0.333	0.367	0.317	0.367	0.350	0.467	0.383	0.367	−0.07
GR	[-]	0.133	0.133	0.250	0.150	0.133	0.133	0.133	0.150	0.150	−1.46
$\dot{m}_{he,st}$	[$kgs^{-1}m^{-2}$]	0.0070	0.0077	0.0077	0.0067	0.0043	0.0083	0.0153	0.0123	0.0110	8.78
T_{melt}	[K]	305	304	297	297	299	306	297	302	294	−0.22
A_{wt}	[m^2m^{-2}]	0.117	0.100	0.050	0.117	0.100	0.150	0.117	0.100	0.100	1.58
$SHGC$	[-]	0.533	0.333	0.400	0.333	0.367	0.400	0.467	0.200	0.167	−7.81
A_{pv}	[m^2m^{-2}]	0.600	0.600	0.600	0.567	0.600	0.500	0.500	0.600	0.567	−1.17

A_{pv} [m^2m^{-2}] is found to be closer to the maximum of the permissible range, 0.1–0.6 [-], suggesting that in the Canadian climate PV is one of the most cost effective approaches to harness green electricity. The optimized swept area of WT A_{wt} [m^2m^{-2}] is found to be closer to the middle of the permissible range, 0.05–0.2 [m^2m^{-2}]. This is influenced by magnitude of wind speed, intermittency of wind, and the associated economics.

Some solutions show sensitivity to climate change scenarios in the future, which can be quantified using the percent change of the optimized solution per decade. Under RCP 4.5 [Wm^{-2}] the five greatest magnitudes of the optimized solution change are associated with V_{pcm} (8.94 [%]), V_{bites} (6.98 [%]), $\dot{m}_{st,f}$ (6.96 [%]), α_R (−4.03 [%]), and $\dot{m}_{he,st}$ (−3.70 [%]). Under RCP 8.5 [Wm^{-2}] the five greatest magnitudes of the optimized solution change are associated with $\dot{m}_{st,f}$ (14.51 [%]), $\dot{m}_{he,st}$ (8.78 [%]), $SHGC$ (−7.81 [%]), V_{pcm} (−4.23 [%]), and A_{ST} (3.70 [%]).

We will attempt to explain the observed trends for the optimized solutions that show the highest sensitivity to the climate change scenario in the future. Fig. 12 shows the optimized roof albedo α_R [-] as it changes for climate change scenarios in the future. On the one hand, higher roof albedos help with reducing the building cooling demand in the Summer season by reflecting the shortwave solar radiation; on the other hand, lower roof albedos help with reducing the building heating demand in the Winter season by absorbing the shortwave solar radiation. The combined effects suggest that lower albedos are desirable, particularly for future climate change scenario of RCP 4.5 [Wm^{-2}].

Fig. 13 shows the optimized Solar Heat Gain Coefficient $SHGC$ [-] as it changes for climate change scenarios in the future. $SHGC$ is a variable that relates to windows. The higher the $SHGC$ the greater amount of solar radiation is absorbed through a window. Again, a lower $SHGC$ helps with reducing the building cooling demand in the Summer season; while, a higher $SHGC$ helps with reducing the building heating demand in the Winter season. The combined effects suggest that a lower $SHGC$ is desirable, particularly for future climate change scenario of RCP 8.5 [Wm^{-2}].

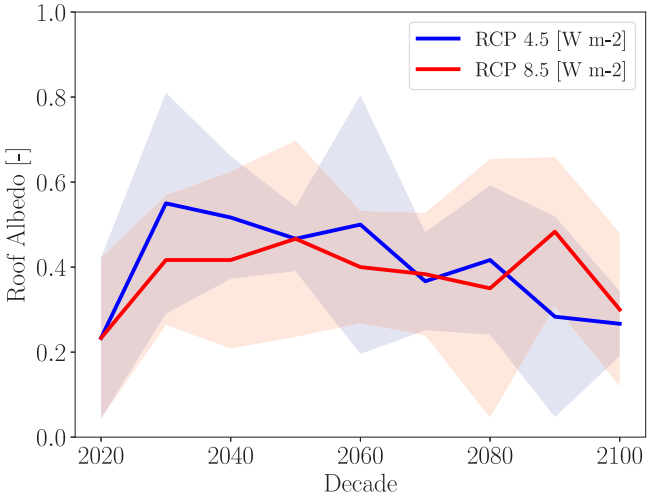

Fig. 12. Optimized roof albedo α_R [-] from 2020 to 2100 under two RCP scenarios of 4.5 and 8.5 [Wm^{-2}]; for the retrofitted case, the average (line) and 1 standard deviation (shaded band) over 3 runs are shown.

Fig. 14 shows the optimized area of solar thermal collector A_{ST} [m^2m^{-2}] as it changes for climate change scenarios in the future. With climate warming, particularly under the RCP 8.5 [Wm^{-2}] scenario, greater amounts of solar thermal collector area can harness the solar thermal energy by 2100. Meanwhile, under the RCP 4.5 [Wm^{-2}] scenario, greater amounts of solar thermal collector area can harness

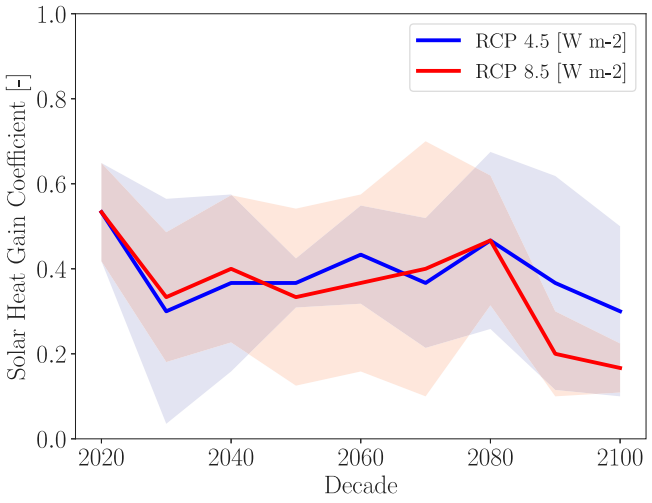

Fig. 13. Optimized Solar Heat Gain Coefficient $SHGC$ [-] from 2020 to 2100 under two RCP scenarios of 4.5 and 8.5 [Wm^{-2}]; for the retrofitted case, the average (line) and 1 standard deviation (shaded band) over 3 runs are shown.

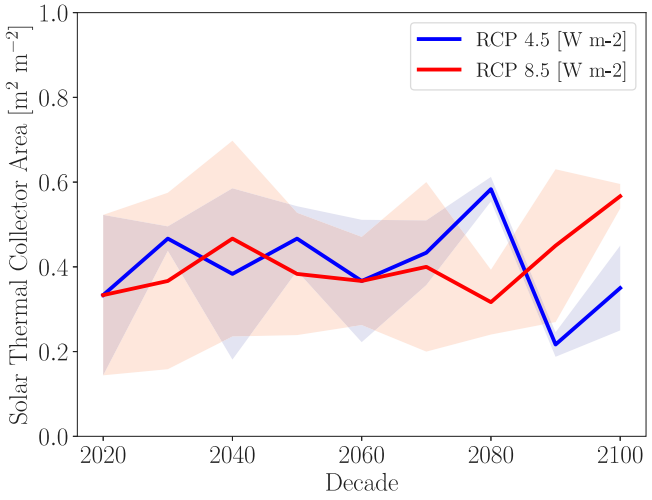

Fig. 14. Optimized area of Solar Thermal collector A_{ST} [m^2m^{-2}] from 2020 to 2100 under two RCP scenarios of 4.5 and 8.5 [Wm^{-2}]; for the retrofitted case, the average (line) and 1 standard deviation (shaded band) over 3 runs are shown.

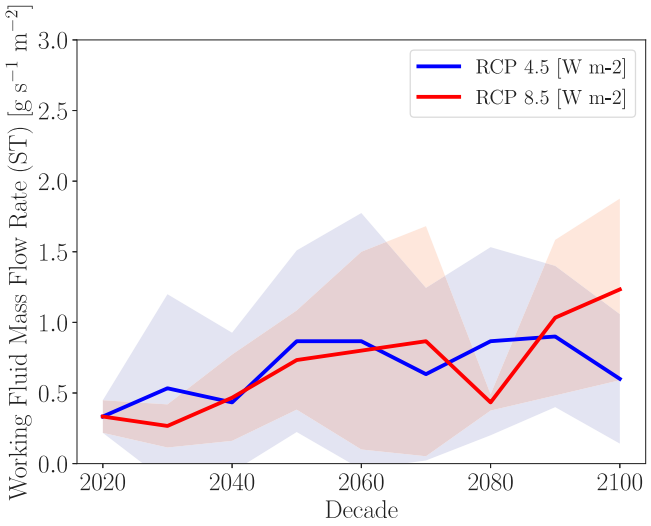

Fig. 15. Optimized mass flow rate of the working fluid in the solar thermal collector $\dot{m}_{st,f}$ [$gs^{-1}m^{-2}$] from 2020 to 2100 under two RCP scenarios of 4.5 and 8.5 [Wm^{-2}]; for the retrofitted case, the average (line) and 1 standard deviation (shaded band) over 3 runs are shown.

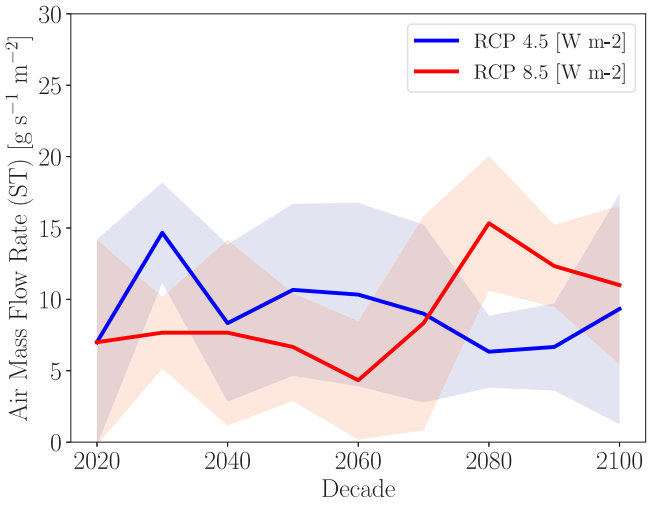

Fig. 16. Optimized mass flow rate of air for the solar thermal collector $\dot{m}_{he,st}$ [$gs^{-1}m^{-2}$] from 2020 to 2100 under two RCP scenarios of 4.5 and 8.5 [Wm^{-2}]; for the retrofitted case, the average (line) and 1 standard deviation (shaded band) over 3 runs are shown.

the solar thermal energy for the warmed decade of 2080, while, lower amounts of solar thermal collector area are recommended for cooled decades of 2090 and 2100.

Related to Fig. 14 are Figs. 15 and 16, which determine how fast solar thermal energy shall by retrieved from the solar thermal collector. With climate warming, particularly under the RCP 8.5 [Wm^{-2}] scenario, greater amounts of mass flow rate of the working fluid in the solar thermal collector $\dot{m}_{st,f}$ [$gs^{-1}m^{-2}$] and mass flow rate of air for the solar thermal collector $\dot{m}_{he,st}$ [$gs^{-1}m^{-2}$] are justified. These flow rates are critical for the optimum performance of the energy system. Mass flow rates that are too low will permit higher temperature gradients to appear between the thermal energy systems, but they do not facilitate flow of heat throughout the thermal energy systems. On the other hand, mass flow rates that are too high will attempt to transfer higher amounts of thermal energy, but they do not permit large enough temperature gradients for effective thermal management.

Figs. 17 and 18 show the optimized volume of Building Integrated Thermal Energy Storage (BITES) system V_{bites} [m^3m^{-2}] and the volume of Phase Change Material (PCM) V_{pcm} [m^3m^{-2}] as they change for climate change scenarios in the future. Under RCP 4.5 [Wm^{-2}] greater amounts of BITES are justified in decades of 2090 and 2100, and greater amounts of PCM are justified in decades of 2060 and 2100. Under RCP 8.5 [Wm^{-2}] greater amounts of BITES are justified in decades of 2030 and 2070, and greater amounts of PCM are justified in decades of 2050 and 2060. Utilization of PCM is mainly triggered in the shoulder seasons, when the temperature of the BITES system oscillates around the melting point of PCM. According to Tables 6 and 7, the optimization process finds appropriate melting temperatures for PCM to range from 294 to 306 [K] given the RCP and decade of interest. Beside finding the appropriate melting temperature, the optimization method uncovers magnitudes of PCM that most appropriately function with the BITES system.

As noted earlier, many of the trends above do not show monotonic increase or decrease from 2020 to 2100. Rather, there is variability in the optimized solutions from one decade to another. This calls for a more detailed optimization that is applied for 20 consecutive years. Doing so, a higher time-resolution trend can be obtained, say from 2020 to 2040, that is appropriate for a particular retrofit study in the

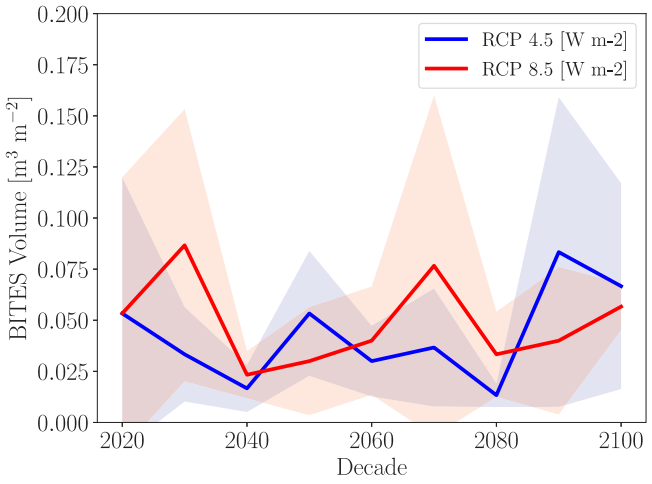

Fig. 17. Optimized volume of Building Integrated Thermal Energy Storage (BITES) system V_{bites} [m^{3}m^{-2}] from 2020 to 2100 under two RCP scenarios of 4.5 and 8.5 [Wm^{-2}]; for the retrofitted case, the average (line) and 1 standard deviation (shaded band) over 3 runs are shown.

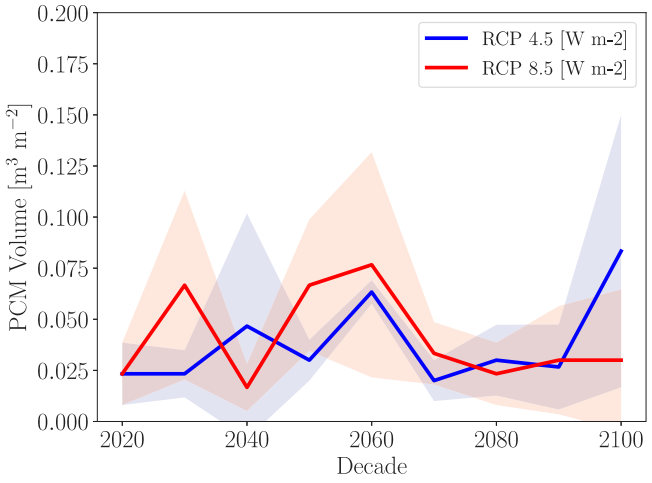

Fig. 18. Optimized volume of Phase Change Material (PCM) V_{pcm} [m^{3}m^{-2}] from 2020 to 2100 under two RCP scenarios of 4.5 and 8.5 [Wm^{-2}]; for the retrofitted case, the average (line) and 1 standard deviation (shaded band) over 3 runs are shown.

near term. The current study, nevertheless, shows the feasibility of conducting the optimization study over any time period of interest or with any time resolution that is desired.

Some controversies also arise from the results found. First, air source heat pumps are criticized for their ineffectiveness in cold climates. They are believed to struggle in the heating season due to outdoor temperatures being too low for effective coefficient of performance and frost problems. However, given the configuration proposed, the heat pump can interact with a thermal energy storage system, for which the temperature can be regulated for effective heat pump performance. In fact, in the VCWG model, the dependence of heat pump coefficient of performance on temperature is accounted for (not shown). Second, there is a misconception that solar thermal technologies are not useful for the cold climates, where high temperatures cannot be reached by solar thermal collectors for water and space heating applications. However, given the configuration proposed, the solar thermal collectors can provide low grade heat, which in combination with the thermal energy storage and heat pump systems can be effective. This is evidenced by optimized solar collector areas that are far greater than the permissible minimum values.

4. Conclusions

Necessitated by the climate change impact of buildings, this study investigates the building retrofit options to reduce the energy consumption of buildings cost-effectively. The study focuses on low-rise two-storey residential houses of Toronto. A particular focus of the study is to propose a building system configuration that is suitable for the cold climate of Canada. The study is framed with a micro-genetic optimization algorithm to size and select numerous building systems to simultaneously reduce electricity consumption, gas consumption, and retrofit cost. The time period considered is from 2020 to 2100 under two Representative Concentration Pathways (RCPs) of 4.5 and 8.5 [Wm^{-2}].

The Vertical City Weather Generator (VCWG v1.5.0) urban physics model is used for building energy and cost calculations for an entire year every decade. The Vatic Weather File Generator (VWFG v1.0.0) is used to create the forcing weather files for VCWG using the statistical down-scaling approach. Beside the standard features, the building systems include a Solar Thermal (ST) collector, Photovoltaic (PV) collector, Wind Turbine (WT), Building Integrated Thermal Energy Storage (BITES) system, Phase Change Material (PCM), Heat Pump (HP), and heat recovery systems in addition to the use of ground thermal energy. The ground-source HP exchanges heat with the building foundation, and it supplements the conventional space heating (natural gas furnace) and cooling (air conditioning) systems. The BITES is charged/discharged using the ST, HP, exhaust air, supply water, or gray water. Fifteen building variables are optimized. These include the volume of BITES, roof albedo, working fluid flow rate for ST, collector area for ST, roof thermal resistance, volume of PCM, infiltration rate, wall thermal resistance, ventilation rate, glazing ratio, air flow rate for ST, melting temperature of PCM, swept area of WT, Solar Heat Gain Coefficient ($SHGC$), and collector area for PV. The following conclusions are reached:

1. Using future climate projections until 2100, future demand for electricity will rise, due to excess cooling demand, and future demand for natural gas will fall, due to a reduction in heating demand.
2. Given the system configuration proposed, the electricity savings are within 39.81–52.68 [%] and 40.40–61.71 [%] for RCPs 4.5 and 8.5 [Wm^{-2}], respectively. The gas savings are within 79.72–82.94 [%] and 80.20–82.67 [%] for RCPs 4.5 and 8.5 [Wm^{-2}], respectively.
3. Compared to standard genetic algorithms, which require many hundreds of iterations to reach a nearly global optimum solution, the micro-genetic optimization algorithm is very efficient and fast, and it reaches a nearly global optimum solution within 30–40 overall iterations.
4. The annualized retrofit cost, about 10–15 thousand Dollars, is not affected substantially by the decades and the future climate change scenario.
5. The retrofitted systems will save large amounts of GreenHouse Gas (GHG) emissions in the range 325–475 [TonnesCO_2] over the duration of 20 years. The GHG emissions savings are greater in the early decades, than the late decades. The GHG emissions savings are greater for the RCP 4.5 [Wm^{-2}] scenario than the RCP 8.5 [Wm^{-2}] scenario.
6. Some optimized building variables do not show sensitivity to time and the future climate change scenario. Specifically, the optimized ventilation/infiltration rates and glazing ratio are found to be closer to the minimum of the permissible ranges. The optimized envelop thermal resistance values (for walls and roof) and swept area of WT, are closer to the middle of the permissible ranges. The optimized PV area is closer to the maximum of the permissible range.

7. Some optimized building variables show sensitivity to time and the future climate change scenario, but they do not show overall trends for the time period 2020–2100. Specifically, the optimum melting temperature for PCM is found to change decade by decade.
8. Some optimized building variables show overall trends for the time period 2020–2100 under the two RCP scenarios. Specifically, under RCP 4.5 [Wm^{-2}], the volume of BITES, the volume of PCM, and working fluid flow rate for ST are suggested to increase, while the roof albedo and air flow rate for ST are suggested to decrease. Under RCP 8.5 [Wm^{-2}], the collector area for ST, working fluid flow rate for ST, and air flow rate for ST are suggested to increase, while the volume of PCM and $SHGC$ are suggested to decrease.
9. For optimized variables with decade-by-decade variability, it is suggested to conduct detailed optimization studies in 20 consecutive years. For practical retrofits under consideration, the increased time-resolution for the optimization study informs stake holders' decisions more appropriately. This clarifies better value choices for the optimized variables.
10. Contrary to popular belief, that solar thermal and heat pump technologies are not suitable for cold climates, there is evidence that such technologies show promise for integration into the building systems for energy and cost savings, given the proposed configuration in this study.

The overall study is successful, showing that the micro-genetic optimization algorithm can find, computationally fast, building system configurations that result in simultaneous electricity consumption, gas consumption, and retrofit cost savings. The limitations of this study inspire future developments:

1. Future work shall entail investigation of other building types (e.g. office buildings, public buildings, commercial buildings, etc.).
2. Future work shall investigate other climate zones in Canada and world-wide.
3. Future work shall increase the time resolution for the optimization study by performing annual simulations continuously for a period of 20–30 years for a targeted retrofit study (i.e. for years 2030, 2031, 2032, etc.).
4. The number of optimization variables may be increased, or new variables may be considered. For instance, currently, the research community is interested in climate impacts of urban vegetation and green building exteriors, which can be studied in the future [62].
5. Future work shall extend the optimization objective functions to parameters describing indoor air quality and thermal comfort as well [13,63].
6. Future work shall study the convergence behavior of genetic algorithms in their ability to reach a nearly global optimum solution given their population size, number of generations, and internal settings. Current research cannot affirm the convergence behavior of such algorithms formally, so fundamental research is needed in this regard.
7. The proposed configuration for the building systems is only one possible scenario adapted for the cold climate of Canada. In future, other building system configurations may be explored using VCWG v1.5.0 or later versions.
8. Beside the operational carbon footprint of buildings, future work shall focus on the embodied carbon footprint of new buildings with a more comprehensive optimization approach.

CRediT authorship contribution statement

Amir A. Aliabadi: Writing – review & editing, Writing – original draft, Visualization, Validation, Supervision, Software, Methodology, Investigation, Funding acquisition, Formal analysis, Data curation. **Xuan Chen:** Writing – review & editing, Software, Methodology, Investigation, Data curation, Conceptualization. **Jiachuan Yang:** Writing – review & editing, Writing – original draft, Supervision, Methodology, Investigation, Funding acquisition. **Ali Madadizadeh:** Writing – review & editing, Investigation, Formal analysis, Data curation. **Kamran Siddiqui:** Writing – review & editing, Writing – original draft, Supervision, Funding acquisition.

Declaration of competing interest

The authors declare that they have no known competing financial interests or personal relationships that could have appeared to influence the work reported in this paper.

Data availability

The Atmospheric Innovations Research (AIR) Laboratory at the University of Guelph provides the model source code. For access, contact Amir A. Aliabadi (aliabadi@uoguelph.ca), visit https://www.aaa-scientists.com/, or visit https://github.com/AmirAAliabadi.

Acknowledgments

The authors thank Rachel Maeve McLeod, Mohsen Moradi, and Jashanpreet Judge who helped processing weather files for the Vatic Weather File Generator (VWFG) and the Vertical City Weather Generator (VCWG). The authors thank William Childs for performing a validation study to compare VCWG building energy consumption output against observed data. The computational platforms were set up with the assistance of Jeff Madge, Joel Best, Matthew Kent, Bogdan Bunescu, and Matthew Kurylo at the University of Guelph. The administrative support from Carolyn Osborn, Shannon MacDonald, Karine Semina, Martha Davies, Suzana Milosevic, Natalie Feil, Jacqueline Floyd, Lauren Fyke, and Piyali Mukherjee Roy is appreciated.

This work was supported by the University of Guelph, Canada through the International Doctoral Tuition Scholarship (IDTS); the Discovery Grant program (401231) from the Natural Sciences and Engineering Research Council (NSERC) of Canada; and the Climate Action and Awareness Fund (CAAF) (055725) from Environment and Climate Change Canada (ECCC).

Appendix

A.1. Retrofitted building systems energy model

The ST collector is modeled using the parameterization of Hottel–Whillier–Bliss [64]. This model is developed for non-building integrated flat plate collectors. This model computes an energy balance that considers the shortwave radiation gain, longwave radiation loss, and convective loss to air at ambient conditions. It determines the available solar energy Q_{st} [Wm^{-2}] for a collector as [64]

$$Q_{st} = FR_{st}A_{st}\left[(\tau\alpha)_e I - U_{st}(T_{st,f,i} - T_a)\right] = \dot{m}_{st,f}c_{st,f}(T_{st,f,o} - T_{st,f,i}), \quad (9)$$

where FR_{st} [-] is the heat removal coefficient, A_{st} [m^2m^{-2}] is the collector area per building footprint area, $(\tau\alpha)_e$ [-] is the effective transmittance–absorbance product, I [Wm^{-2}] is the incoming shortwave radiation flux normal to the collector, U_{st} [$Wm^{-2}K^{-1}$] is the convective and radiative heat loss factor, $T_{st,f,i}$ [K] is the inlet working fluid temperature to the collector, $T_{st,f,o}$ [K] is the outlet working fluid

temperature from the collector, T_a [K] is outdoor atmospheric temperature, $\dot{m}_{st,f}$ [kgs^{-1}m^{-2}] is the mass flow rate of the working fluid through the collector per unit building footprint area, and $c_{st,f}$ [Jkg^{-1}K^{-1}] is the heat capacity of the working fluid at constant pressure. The incident shortwave radiation flux normal to the collector I [Wm^{-2}] is calculated by [5,65]

$$I = S^{\downarrow dir}\cos\theta_a\cos(\theta_z - \beta_{st}) + S^{\downarrow diff}, \tag{10}$$

where β_{st} [°] is the collector tilt angle, θ_z [°] the zenith angle, θ_a [°] the azimuth angle, $S^{\downarrow dir}$ [Wm^{-2}] is the direct shortwave radiation flux vector from the sky, and $S^{\downarrow diff}$ [Wm^{-2}] is the diffuse shortwave radiation flux vector from the sky.

The electric power output of the PV panel is computed assuming a constant conversion efficiency such that [65]

$$W_{pv} = \eta_{pv}A_{pv}I = \eta_{pv}A_{pv}S^{\downarrow dir}\cos\theta_a\cos(\theta_z - \beta_{pv}), \tag{11}$$

where A_{pv} [m^{2}m^{-2}] is the collector area per building footprint area, η_{pv} [-] is conversion efficiency, and β_{pv} [°] is the tilt angle of the PV system, which is usually considered close to the latitude angle at the site of interest.

The electric power output of the WT system is computed using the most generic WT equation, for a specified operational range of minimum and maximum possible wind speeds, such that [66]

$$W_{wt} = 0.5\eta_{wt}\rho A_{wt}S^3, \tag{12}$$

where η_{wt} [-] is the turbine efficiency, ρ [kgm^{-3}] is air density, and S [ms^{-1}] is wind speed near roof level of a building, and A_{wt} [m^{2}m^{-2}] is swept area of the turbine per building footprint area.

The counter-flow heat exchanger is used to exchange thermal energy between the ST collector (working fluid) and the BITES (air) systems. The goal of the heat exchanger model is to find a relationship between inlet and outlet temperatures for the two streams of the fluids. This relationship can be given using the efficiency of the heat exchanger

$$\eta_{he,st} = \frac{T_{st,f,o} - T_{st,f,i}}{T_{st,f,o} - T_{he,st,i}}. \tag{13}$$

We can provide an equation for $T_{he,st,o}$ [K] given other inlet temperatures ($T_{st,f,o}$ and $T_{he,st,i}$ [K]), mass flow rates ($\dot{m}_{st,f}$ and $\dot{m}_{he,st}$ [kgs^{-1}m^{-2}]), and heat capacities ($c_{st,f}$ and c_{air} [Jkg^{-1}K^{-1}])

$$\begin{aligned} T_{he,st,o} - T_{he,st,i} &= \frac{\dot{m}_{st,f}c_{st,f}}{\dot{m}_{he,st}c_{air}}(T_{st,f,o} - T_{st,f,i}),\\ &= \frac{\dot{m}_{st,f}c_{st,f}}{\dot{m}_{he,st}c_{air}}\eta_{he,st}(T_{st,f,o} - T_{he,st,i}),\\ T_{he,st,o} &= \frac{\dot{m}_{st,f}c_{st,f}}{\dot{m}_{he,st}c_{air}}\eta_{he,st}(T_{st,f,o} - T_{he,st,i}) + T_{he,st,i}. \end{aligned} \tag{14}$$

We use a lump system approach with uniform temperature T_{bites} [K] for the BITES system. Given the sensible energy balance, the change in temperature of the BITES system over finite time Δt [s], considering heat gains $Q_{gain,i}$ [Wm^{-2}], heat losses $Q_{loss,i}$ [Wm^{-2}], and ground heat transfer Q_{ground} [Wm^{-2}] can be written as

$$\Delta T_{bites}V_{bites}c_{bites} = +\sum_{i=1}^{n}Q_{gain,i}\Delta t - \sum_{i=1}^{m}Q_{loss,i}\Delta t + Q_{ground}\Delta t, \tag{15}$$

where ΔT_{bites} [K] is change in the temperature of the BITES system, V_{bites} [m^{3}m^{-2}] is the volume of the BITES system per unit building footprint area, and c_{bites} [Jm^{-3}K^{-1}] is the volumetric heat capacity of the BITES system. The BITES system may be simultaneously charged or discharged using multiple sources and/or sinks of energy. The temperatures of the surrounding systems determine the availability of heat gains and losses for the BITES system.

The ground heat flux is calculated using the resistance R_{deep} [m^{2}KW^{-1}] between the BITES temperature T_{bites} [K] and the deep soil temperature T_{deep} [K]. The ground heat flux could act as a source (heating BITES) or sink (cooling BITES) of thermal energy for the BITES system. The ground heat flux can be given as

$$Q_{ground} = \frac{T_{deep} - T_{bites}}{R_{deep}}. \tag{16}$$

If PCMs are embedded in the BITES system, the heat transferred to the material results in melting or solidifying a portion of the volume of PCM without changing the temperature of the BITES system. The latent heat balance equation for the PCM can be given as

$$\Delta V_{pcm}l_{pcm} = +\sum_{i=1}^{n}Q_{gain,i}\Delta t - \sum_{i=1}^{m}Q_{loss,i}\Delta t + Q_{ground}\Delta t, \tag{17}$$

where ΔV_{pcm} [m^{3}m^{-2}] is the change in volume of PCM melted (positive) or solidified (negative) per unit building footprint area and l_{pcm} [Jm^{-3}] is the volumetric latent heat of melting/solidification.

The HP equations can be developed using the first law of thermodynamics. This law states that the electricity consumption (W_{hp}) in addition to the heat removed from a cold reservoir of heat (Q_L) should be equal to the heat forced into a warm reservoir of heat (Q_H). The COP_{hp} for the HP is defined differently under heating or cooling modes. The following three equations are used [67]

$$W_{hp} + Q_L = Q_H, \tag{18}$$

$$COP_{hp} = \frac{Q_H}{W_{hp}}\ \text{(Heating mode)}, \tag{19}$$

$$COP_{hp} = \frac{Q_L}{W_{hp}}\ \text{(Cooling mode)}. \tag{20}$$

In fact, the COP_{hp} of the heat pump is characterized by a performance curve that considers the effect of outside temperature. The COP_{hp} is adjusted using this performance curve, such that it varies from 1.5 to 4 for outside temperatures from 253.15 [K] to 308.15 [K], respectively [67].

A.2. Economics model

The marginal annualized cost of a building systems retrofit is given by

$$C = C_I + C_G + C_E + C_{OM} - C_S, \tag{21}$$

where C_I is the annualized initial investment for the systems' acquisition, C_G is the annualized cost of fuel consumption (natural gas in this study), C_E is the annualized cost of electricity consumption supplied from the grid, C_{OM} is the annualized cost of operation and maintenance, and C_S is the annualized income of discarding the systems (salvage value). These costs are calculated for a residential two-storey building assuming a building footprint area of 196 [m^2], building wall area of 336 [m^2], and building roof area of 271 [m^2] that is pitched.

The goal of the economic analysis is to know the *marginal* annualized cost, defined as the difference in cost for a retrofitted building system and a pre-existing system. Without retrofitting the building, the marginal initial cost for a conventional system is C_B [$]. This cost is not zero because without retrofitting the building the conventional system would be over-sized to meet the energy demand. This annualized cost can be given by [5,65]

$$C_{IB} = C_B \times CRF(i, N). \tag{22}$$

The capital recovery factor calculates the annualized payment required to form a total present worth of an amount given a discounting rate (here the effective interest rate i) and the number of years N = 20. The capital recovery factor and effective interest rate are given by [5,65]

$$CRF(i, N) = \frac{i}{1 - (1 + i)^{-N}}, \tag{23}$$

$$i = \frac{i_n - j}{1 + j}, \tag{24}$$

Table 8
Parameters required for the economic analysis.
Source: Values adapted from Aliabadi et al. [5].

Parameter	Units	Description	Value
i_n	[%]	Nominal interest rate	3.78
j	[%]	Inflation rate	1.88
P_G	[$\$m^{-3}$]	Natural gas price	0.137
j_G	[%]	Natural gas price increase	1.00
P_E	[$\$kW-hr^{-1}$]	Electricity price	0.127
j_E	[%]	Electricity price increase	4.50
P_{pv}	[$\$m^{-2}$]	Price of photovoltaic collector	377
P_{wt}	[$\$m^{-2}$]	Price of wind turbine	490 × 2[a]
P_{st}	[$\$m^{-2}$]	Price of solar thermal collector	340
P_{bites}	[$\$m^{-3}$]	Price of BITES	200
P_{pcm}	[$\$m^{-3}$]	Price of PCM	1930 × 2[a]
P_{hp}	[$\$m^{-2}$]	Price of heat pump	20 × 2[a]
P_{wall}	[$\$m^{-4}K^{-1}W$]	Price of increasing thermal resistance	8
P_{roof}	[$\$m^{-4}K^{-1}W$]	Price of increasing thermal resistance	8
ITC_{pv}	[$]	Rebate for photovoltaic collector	3000
ITC_{inf}	[$]	Rebate for air tightness	550
ITC_R	[$\$m^{-4}K^{-1}W$]	Rebate for thermal resistance	2.15
C_{OMB}	[$\$m^{-2}$]	Operation and maintenance for base system	1
OM_{pv}	[$\$m^{-2}$]	Operation and maintenance for photovoltaic collector	$0.01P_{pv}$
OM_{wt}	[$\$m^{-2}$]	Operation and maintenance for wind turbine	$0.02P_{wt}$
OM_{st}	[$\$m^{-2}$]	Operation and maintenance for solar thermal collector	$0.01P_{st}$
OM_{bite}	[$\$m^{-3}$]	Operation and maintenance for BITES	$0.01P_{bites}$
OM_{pcm}	[$\$m^{-3}$]	Operation and maintenance for PCM	$0.01P_{pcm}$
OM_{hp}	[$\$m^{-2}$]	Operation and maintenance for heat pump	$0.05P_{hp}$
OM_{cr}	[$]	Operation and maintenance for cool roof	75
F_{SB}	[-]	Salvage factor for base system	0.03
F_S	[-]	Salvage factor for renewable energy system	0.05
C_B	[$\$m^{-2}$]	Marginal initial cost for base system	5

[a]Systems that require one replacement over the investment horizon.

where i_n is the nominal interest rate and j is the inflation rate. The interest rate $i_n = 0.0378$ is taken as the median value of the prime rate over the last 20 years by Statistics Canada.[2] The inflation rate $j = 0.0188$ is also taken as the median value over the last 20 years.[3]

The annualized initial investment for retrofitted building systems can be calculated by adding the initial price, subtracting the government rebate (or incentive), and annualizing the cost using

$$\begin{aligned} C_I = [&A_{pv}P_{pv} + A_{wt}P_{wt} + A_{st}P_{st} + V_{bites}P_{bites} \\ &+ V_{pcm}P_{pcm} + A_{cr}P_{cr} + A_{bld}P_{hp} + P_{inf} + P_{env} \\ &- ITC_{pv} - ITC_{inf} - A_{wall}\Delta R_{wall}ITC_R \\ &- A_{roof}\Delta R_{roof}ITC_R] \times CRF(i,N), \end{aligned} \tag{25}$$

where P_k is the unit installation cost for a given system. For PV collectors P_{pv} [$\$m^{-2}$] is given per unit collector area; for WT P_{wt} [$\$m^{-2}$] is given per unit swept area of wind; for ST collectors P_{st} [$\$m^{-2}$] is given per unit collector area; for BITES P_{bites} [$\$m^{-3}$] is given per unit volume; for PCM P_{pcm} [$\$m^{-3}$] is given per unit volume; for cool roofs P_{cr} [$\$m^{-2}$] is given per unit roof area; for HP P_{hp} [$\$m^{-2}$] is given per unit building footprint area; for infiltration/exfiltration P_{inf} [$] is a one time cost for improving the air tightness; for the building envelop P_{env} [$] is calculated by knowing the price associated with increasing the thermal resistance of walls and roofs such that

$$P_{env} = A_{wall}\Delta R_{wall}P_{wall} + A_{roof}\Delta R_{roof}P_{roof}, \tag{26}$$

where P_{wall} and P_{roof} [$\$m^{-4}K^{-1}W$] are the prices for increasing thermal resistance values for the wall and roof. The rebates for building system retrofits are given by ITC_{pv} [$] for PV, ITC_{inf} [$] for reducing building infiltration/exfiltration by improving air tightness, and ITC_R [$\$m^{-4}K^{-1}W$] by increasing the thermal resistance values of the envelop.

The annualized cost of fuel consumption (natural gas), for both the base and retrofitted systems, should be calculated by factoring in the annual rate of increase in fuel price j_G and the present worth factor $PWF(i,k)$, given by [5,65]

$$C_{GB} = \left(\sum_{k=1}^{N} A_{bld}(G_{hB} + G_{whB})P_G(1+j_G)^k PWF(i,k)\right) CRF(i,N), \tag{27}$$

$$C_G = \left(\sum_{k=1}^{N} A_{bld}(G_h + G_{wh})P_G(1+j_G)^k PWF(i,k)\right) CRF(i,N), \tag{28}$$

$$PWF(i,k) = \frac{1}{(1+i)^k}, \tag{29}$$

where G_{hB} and G_{whB} [m^3m^{-2}] are total annual gas consumption per building footprint area required for space and water heating of the base case, respectively, G_h and G_{wh} [m^3m^{-2}] are total annual gas consumption per building footprint area required for space and water heating of the retrofitted system, respectively, and P_G [$\$m^{-3}$] is the current fuel price per cubic meter at standard pressure.

The annualized cost of electricity consumption for the base system should be calculated by factoring in the annual rate of increase in electricity price j_E

$$C_{EB} = \left(\sum_{k=1}^{N} A_{bld}(E_{cB} + E_{dB})P_E(1+j_E)^k PWF(i,k)\right) CRF(i,N), \tag{30}$$

where E_{cB} and E_{dB} [$kW-hrm^{-2}$] are total annual electricity consumption per building footprint area required for space cooling and domestic use of the base case, respectively, and P_E [$\$kW-hr^{-1}$] is the current electricity price.

The annualized cost of electricity consumption for the retrofitted system should consider more terms that relate to electricity required for heating by the HP E_h [$kW-hrm^{-2}$] and electricity generated by the PV collector E_{pv} [$kW-hrm^{-2}$] and WT E_{wt} [$kW-hrm^{-2}$] such that

$$\begin{aligned} C_E = \Bigg(&\sum_{k=1}^{N} A_{bld}(E_h + E_c + E_d - E_{pv} - E_{wt}) \times P_E \\ &\times (1+j_E)^k \times PWF(i,k)\Bigg) CRF(i,N). \end{aligned} \tag{31}$$

[2] www150.statcan.gc.ca/ (accessed 13 March 2023).
[3] https://www.macrotrends.net/countries/CAN/canada/inflation-rate-cpi/ (accessed 13 March 2023).

The annualized marginal cost of operation and maintenance for the base system is set to $C_{OMB} = 1$ [$\$m^{-2}$], which is lower than the same cost for the retrofitted system, given by

$$C_{OM} = A_{pv}OM_{pv} + A_{wt}OM_{wt} + A_{st}OM_{st} + V_{bites}OM_{bites} + V_{pcm}OM_{pcm} + A_{bld}OM_{hp} + OM_{cr}, \quad (32)$$

where OM_{pv} [$\$m^{-2}$] is operation and maintenance cost for the PV system per unit panel area; OM_{wt} [$\$m^{-2}$] is cost for WT per unit swept area of wind; OM_{st} [$\$m^{-2}$] is cost for ST collector per unit collector area; OM_{bites} [$\$m^{-3}$] is cost for BITES per unit volume; OM_{pcm} [$\$m^{-3}$] is cost for PCM per unit volume; OM_{hp} [$\$m^{-2}$] is cost for HP per unit building footprint area; and OM_{cr} [$] is cost of repair for the cool roof.

The annualized revenue by salvaging the building components can be calculated by assuming a salvage factor, F_{SB} or F_S for the base and retrofitted systems, respectively, and applying the $PWF(i,N)$ and $CRF(i,N)$ for the full period of N years

$$C_{SB} = F_{SB} \times C_{IB} \times PWF(i,N) \times CRF(i,N), \quad (33)$$

$$C_S = F_S \times C_I \times PWF(i,N) \times CRF(i,N). \quad (34)$$

Table 8 shows the constants used in the economic analysis. The values are retrieved and justified from a study by Aliabadi et al. [5].

References

[1] G. Kim, H.S. Lim, T.S. Lim, L. Schaefer, J.T. Kim, Comparative advantage of an exterior shading device in thermal performance for residential buildings, Energy Build. 46 (2012) 105–111, http://dx.doi.org/10.1016/j.enbuild.2011.10.040.

[2] A.J. Cannon, D.I. Jeong, X. Zhang, F.W. Zwiers, Climate-Resilient Buildings and Core Public Infrastructure: An Assessment of the Impact of Climate Change on Climatic Design Data in Canada, Technical Report, Environment and Climate Change Canada, Ottawa, 2020.

[3] J. Mukkavaara, F. Shadram, An integrated optimization and sensitivity analysis approach to support the life cycle energy trade-off in building design, Energy Build. 253 (2021) 111529, http://dx.doi.org/10.1016/j.enbuild.2021.111529.

[4] M. Bilardo, M. Ferrara, E. Fabrizio, Performance assessment and optimization of a solar cooling system to satisfy renewable energy ratio (RER) requirements in multi-family buildings, Renew. Energy 155 (2020) 990–1008, http://dx.doi.org/10.1016/j.renene.2020.03.044.

[5] A.A. Aliabadi, M. Moradi, R.M. McLeod, D. Calder, R. Dernovsek, How much building renewable energy is enough? The vertical city weather generator (VCWG v1.4.4), Atmosphere 12 (7) (2021) 882, http://dx.doi.org/10.3390/atmos12070882.

[6] M. Wetter, J. Wright, A comparison of deterministic and probabilistic optimization algorithms for nonsmooth simulation-based optimization, Build. Environ. 39 (8) (2004) 989–999, http://dx.doi.org/10.1016/j.buildenv.2004.01.022.

[7] J.H. Kämpf, M. Wetter, D. Robinson, A comparison of global optimization algorithms with standard benchmark functions and real-world applications using EnergyPlus, J. Build. Perform. Simul. 3 (2) (2010) 103–120, http://dx.doi.org/10.1080/19401490903494597.

[8] R.T. Marler, J.S. Arora, The weighted sum method for multi-objective optimization: new insights, Struct. Multidiscip. Optim. 41 (6) (2010) 853–862.

[9] K. Bamdad, M.E. Cholette, L. Guan, J. Bell, Building energy optimisation under uncertainty using ACOMV algorithm, Energy Build. 167 (2018) 322–333, http://dx.doi.org/10.1016/j.enbuild.2018.02.053.

[10] K. Bamdad, M.E. Cholette, S. Omrani, J. Bell, Future energy-optimised buildings — Addressing the impact of climate change on buildings, Energy Build. 231 (2021) 110610, http://dx.doi.org/10.1016/j.enbuild.2020.110610.

[11] J. Wang, H. Chen, Y. Yuan, Y. Huang, A novel efficient optimization algorithm for parameter estimation of building thermal dynamic models, Build. Environ. 153 (2019) 233–240, http://dx.doi.org/10.1016/j.buildenv.2019.02.006.

[12] S. Park, S.K. Park, A micro-genetic algorithm (GA v1.7.1a) for combinatorial optimization of physics parameterizations in the Weather Research and Forecasting model (v4.0.3) for quantitative precipitation forecast in Korea, Geosci. Model Dev. 14 (10) (2021) 6241–6255, http://dx.doi.org/10.5194/gmd-14-6241-2021.

[13] H.B. Gunay, M. Ouf, G. Newsham, W. O'Brien, Sensitivity analysis and optimization of building operations, Energy Build. 199 (2019) 164–175, http://dx.doi.org/10.1016/j.enbuild.2019.06.048.

[14] D. Tuhus-Dubrow, M. Krarti, Genetic-algorithm based approach to optimize building envelope design for residential buildings, Build. Environ. 45 (7) (2010) 1574–1581, http://dx.doi.org/10.1016/j.buildenv.2010.01.005.

[15] A. Moazami, V.M. Nik, S. Carlucci, S. Geving, Impacts of future weather data typology on building energy performance – investigating long-term patterns of climate change and extreme weather conditions, Appl. Energy 238 (2019) 696–720, http://dx.doi.org/10.1016/j.apenergy.2019.01.085.

[16] L. Troup, M.J. Eckelman, D. Fannon, Simulating future energy consumption in office buildings using an ensemble of morphed climate data, Appl. Energy 255 (2019) 113821, http://dx.doi.org/10.1016/j.apenergy.2019.113821.

[17] G. Fraisse, K. Johannes, V. Trillat-Berdal, G. Achard, The use of a heavy internal wall with a ventilated air gap to store solar energy and improve summer comfort in timber frame houses, Energy Build. 38 (4) (2006) 293–302, http://dx.doi.org/10.1016/j.enbuild.2005.06.010.

[18] Y. Chen, A.K. Athienitis, K. Galal, Modeling, design and thermal performance of a BIPV/T system thermally coupled with a ventilated concrete slab in a low energy solar house: Part 1, BIPV/T system and house energy concept, Sol. Energy 84 (11) (2010) 1892–1907, http://dx.doi.org/10.1016/j.solener.2010.06.013.

[19] Y. Chen, K. Galal, A.K. Athienitis, Modeling, design and thermal performance of a BIPV/T system thermally coupled with a ventilated concrete slab in a low energy solar house: Part 2, ventilated concrete slab, Sol. Energy 84 (11) (2010) 1908–1919, http://dx.doi.org/10.1016/j.solener.2010.06.012.

[20] A. Fallahi, F. Haghighat, H. Elsadi, Energy performance assessment of double-skin façade with thermal mass, Energy Build. 42 (9) (2010) 1499–1509, http://dx.doi.org/10.1016/j.enbuild.2010.03.020.

[21] F.M. Rad, A.S. Fung, W.H. Leong, Feasibility of combined solar thermal and ground source heat pump systems in cold climate, Canada, Energy Build. 61 (2013) 224–232, http://dx.doi.org/10.1016/j.enbuild.2013.02.036.

[22] R. Kamel, N. Ekrami, P. Dash, A. Fung, G. Hailu, BIPV/T+ASHP: Technologies for NZEBs, Energy Procedia 78 (2015) 424–429, http://dx.doi.org/10.1016/j.egypro.2015.11.687.

[23] J.M. Tardif, J. Tamasauskas, V. Delisle, M. Kegel, Performance of air based BIPV/T heat management strategies in a Canadian home, Procedia Environ. Sci. 38 (2017) 140–147, http://dx.doi.org/10.1016/j.proenv.2017.03.095, Sustainable synergies from Buildings to the Urban Scale.

[24] D. Connolly, H. Lund, B. Mathiesen, M. Leahy, A review of computer tools for analysing the integration of renewable energy into various energy systems, Appl. Energy 87 (4) (2010) 1059–1082, http://dx.doi.org/10.1016/j.apenergy.2009.09.026.

[25] V. Harish, A. Kumar, A review on modeling and simulation of building energy systems, Renew. Sustain. Energy Rev. 56 (2016) 1272–1292, http://dx.doi.org/10.1016/j.rser.2015.12.040.

[26] B. Bueno, L.K. Norford, G. Pigeon, R. Britter, Combining a detailed building energy model with a physically-based urban canopy model, Bound.-Lay. Meteorol. 140 (3) (2011) 471–489, http://dx.doi.org/10.1007/s10546-011-9620-6.

[27] B. Bueno, L. Norford, J. Hidalgo, G. Pigeon, The urban weather generator, J. Build. Perform. Simul. 6 (4) (2012) 269–281, http://dx.doi.org/10.1080/19401493.2012.718797.

[28] B. Bueno, G. Pigeon, L.K. Norford, K. Zibouche, C. Marchadier, Development and evaluation of a building energy model integrated in the TEB scheme, Geosci. Model Dev. 5 (3) (2012) 433–448, http://dx.doi.org/10.5194/gmd-5-433-2012.

[29] B. Bueno, M. Roth, L.K. Norford, R. Li, Computationally efficient prediction of canopy level urban air temperature at the neighbourhood scale, Urban Clim. 9 (2014) 35–53, http://dx.doi.org/10.1016/j.uclim.2014.05.005.

[30] M. Moradi, B. Dyer, A. Nazem, M.K. Nambiar, M.R. Nahian, B. Bueno, C. Mackey, S. Vasanthakumar, N. Nazarian, E.S. Krayenhoff, L.K. Norford, A.A. Aliabadi, The Vertical City Weather Generator (VCWG v1.3.2), Geosci. Model Dev. 14 (2) (2021) 961–984, http://dx.doi.org/10.5194/gmd-14-961-2021.

[31] M. Moradi, E.S. Krayenhoff, A.A. Aliabadi, A comprehensive indoor–outdoor urban climate model with hydrology: The Vertical City Weather Generator (VCWG v2.0.0), Build. Environ. 207 (2022) 108406, http://dx.doi.org/10.1016/j.buildenv.2021.108406.

[32] A. Katal, M. Mortezazadeh, L.L. Wang, Modeling building resilience against extreme weather by integrated CityFFD and CityBEM simulations, Appl. Energy 250 (2019) 1402–1417, http://dx.doi.org/10.1016/j.apenergy.2019.04.192.

[33] NRCan, National Energy Use Database, Technical Report, Office of Energy Efficiency, Natural Resources Canada, Gatineau, QC, 2020.

[34] Passive-House-Institute, Criteria for the Passive House EnerPHit and PHI Low Energy Building Standard, Technical Report, Passive House Institute, Darmstadt, 2015.

[35] Active-House, The Active House Specifications, third ed., Active House, The Hague, 2019.

[36] L. Goetz, Quantifying Building Performance in Nine High-Performance Single-Family Houses in Ontario, Canada Master's thesis, Toronto Metropolitan University, Toronto, 2022.

[37] H.-O. Pörtner, D.C. Roberts, H. Adams, et al., Technical summary, in: H.-O. Pörtner, D.C. Roberts, E.S. Poloczanska, et al. (Eds.), Climate Change 2022: Impacts, Adaptation and Vulnerability. Contribution of Working Group II To the Sixth Assessment Report of the Intergovernmental Panel on Climate Change, Cambridge University Press, Cambridge and New York, 2022, pp. 37–118, http://dx.doi.org/10.1017/9781009325844.002.

[38] N. Ekrami, A. Garat, A.S. Fung, Thermal analysis of Insulated Concrete Form (ICF) walls, Energy Procedia 75 (2015) 2150–2156, http://dx.doi.org/10.1016/j.egypro.2015.07.353.

[39] M. Pomianowski, P. Heiselberg, R.L. Jensen, Dynamic heat storage and cooling capacity of a concrete deck with PCM and thermally activated building system, Energy Build. 53 (2012) 96–107, http://dx.doi.org/10.1016/j.enbuild.2012.07.007.

[40] Ontario, Ontario Regulation 541/05: Net Metering, Technical Report, Ontario Energy Board Act, 1998, Toronto, 2022.

[41] L. Bergia Boccardo, O.B. Kazanci, J. Quesada Allerhand, B.W. Olesen, Economic comparison of TABS, PCM ceiling panels and all-air systems for cooling offices, Energy Build. 205 (2019) 109527, http://dx.doi.org/10.1016/j.enbuild.2019.109527.

[42] A.A. Aliabadi, R.M. McLeod, The vatic weather file generator (VWFG v1.0.0), J. Build. Eng. 67 (2023) 105966, http://dx.doi.org/10.1016/j.jobe.2023.105966.

[43] S.E. Belcher, J.N. Hacker, D.S. Powell, Constructing design weather data for future climates, Build. Serv. Eng. Res. Technol. 26 (1) (2005) 49–61, http://dx.doi.org/10.1191/0143624405bt112oa.

[44] A. Afshari, Optimization of urban design/retrofit scenarios using a computationally light standalone urban energy/climate model (SUECM) forced by ERA5 data, Energy Build. 287 (2023) 112991, http://dx.doi.org/10.1016/j.enbuild.2023.112991.

[45] J.F. Scinocca, V.V. Kharin, Y. Jiao, M.W. Qian, M. Lazare, L. Solheim, G.M. Flato, S. Biner, M. Desgagne, B. Dugas, Coordinated global and regional climate modeling, J. Clim. 29 (1) (2016) 17–35, http://dx.doi.org/10.1175/JCLI-D-15-0161.1.

[46] H. Singh, M.R. Najafi, A. Cannon, Evaluation and joint projection of temperature and precipitation extremes across Canada based on hierarchical Bayesian modelling and large ensembles of regional climate simulations, Weather Clim. Extrem. 36 (2022) 100443, http://dx.doi.org/10.1016/j.wace.2022.100443.

[47] A. Amengual, V. Homar, R. Romero, S. Alonso, C. Ramis, A statistical adjustment of regional climate model outputs to local scales: Application to Platja de Palma, Spain, J. Clim. 25 (3) (2012) 939–957, http://dx.doi.org/10.1175/JCLI-D-10-05024.1.

[48] M. Zhu, Y. Pan, Z. Huang, P. Xu, An alternative method to predict future weather data for building energy demand simulation under global climate change, Energy Build. 113 (2016) 74–86, http://dx.doi.org/10.1016/j.enbuild.2015.12.020.

[49] M. Hosseini, A. Bigtashi, B. Lee, A systematic approach in constructing typical meteorological year weather files using machine learning, Energy Build. 226 (2020) 110375, http://dx.doi.org/10.1016/j.enbuild.2020.110375.

[50] M. Hosseini, A. Bigtashi, B. Lee, Generating future weather files under climate change scenarios to support building energy simulation - A machine learning approach, Energy Build. 230 (2021) 110543, http://dx.doi.org/10.1016/j.enbuild.2020.110543.

[51] NRCan, National Energy Code of Canada, Technical Report, Office of Energy Efficiency, Natural Resources Canada, Gatineau, QC, 2017.

[52] ASHRAE, Standard 62.1: Ventilation and Acceptable Indoor Air Quality, Technical Report, American Society for Heating Refrigeration and Airconditioning Engineers, Peachtree Corners, 2022.

[53] ASHRAE, Standard 62.2: Ventilation and Acceptable Indoor Air Quality in Residential Buildings, Technical Report, American Society for Heating Refrigeration and Airconditioning Engineers, Peachtree Corners, 2022.

[54] ASHRAE, Standard 90.1: Energy Standard for Buildings Except Low-Rise Residential Buildings, Technical Report, American Society for Heating Refrigeration and Airconditioning Engineers, Peachtree Corners, 2013.

[55] ASHRAE, Standard 90.2: Energy-Efficient Design of Low-Rise Residential Buildings, Technical Report, American Society for Heating Refrigeration and Airconditioning Engineers, Peachtree Corners, 2018.

[56] ASHRAE, Standard 140: Standard Method of Test for the Evaluation of Building Energy Analysis Computer Programs, Technical Report, American Society for Heating Refrigeration and Airconditioning Engineers, Peachtree Corners, 2017.

[57] R.H. Henninger, M.J. Witte, EnergyPlus Testing with ANSI/ASHRAE Standard 140-2001 (BESTEST), Technical Report, Ernest Orlando Lawrence Berkeley National Laboratory, Berkeley, 2004.

[58] ASHRAE, Guideline 14: Measurement of Energy, Demand, and Water Savings, Technical Report, American Society for Heating Refrigeration and Airconditioning Engineers, Peachtree Corners, 2014.

[59] B. Bueno Unzeta, Study and Prediction of the Energy Interactions Between Buildings and the Urban Climate (Ph.D. thesis), Massachusetts Institute of Technology, Cambridge, 2012.

[60] A.A. Aliabadi, Turbulence: A Fundamental Approach for Scientists and Engineers, Springer, Cham, 2022, http://dx.doi.org/10.1007/978-3-030-95411-6.

[61] A.A. Aliabadi, S.N. Rogak, K.H. Bartlett, S.I. Green, Preventing airborne disease transmission: Review of methods for ventilation design in health care facilities, Adv. Prev. Med. 2011 (2011) 124064, http://dx.doi.org/10.4061/2011/124064.

[62] A. Afshari, A new model of urban cooling demand and heat island—application to vertical greenery systems (VGS), Energy Build. 157 (2017) 204–217, http://dx.doi.org/10.1016/j.enbuild.2017.01.008.

[63] B. Dyer, M. Biglarbegian, A.A. Aliabadi, The autonomous robotic environmental sensor (ARES), Sci. Technol. Built Environ. 27 (10) (2021) 1461–1472, http://dx.doi.org/10.1080/23744731.2021.1971034.

[64] C.C. Smith, T.A. Weiss, Design application of the Hottel–Whillier–Bliss equation, Sol. Energy 19 (2) (1977) 109–113, http://dx.doi.org/10.1016/0038-092X(77)90047-0.

[65] A.A. Aliabadi, J.S. Wallace, Cost-effective and reliable design of a solar thermal power plant, T. Can. Soc. Mech. Eng. 33 (1) (2009) 25–37, http://dx.doi.org/10.1139/tcsme-2009-0004.

[66] B. Dongre, R.K. Pateriya, Power curve model classification to estimate wind turbine power output, Wind Eng. 43 (3) (2019) 213–224, http://dx.doi.org/10.1177/0309524X18780393.

[67] NRCan, Heating and Cooling with a Heat Pump, Technical Report, Office of Energy Efficiency, Natural Resources Canada, Gatineau, QC, 2004.